MICROSTRUCTURAL EVOLUTION AND CORROSION BEHAVIOR OF FeCoNiCrVZr HIGH ENTROPY ALLOYS

M.Tech. Thesis

By

RHISHIKESH DARSHAN

DEPARTMENT OF METALLURGY ENGINEERING AND MATERIALS SCIENCE

INDIAN INSTITUTE OF TECHNOLOGY INDORE

JUNE,2020

MICROSTRUCTURAL EVOLUTION AND CORROSION BEHAVIOR OF FeCoNiCrVZr HIGH ENTROPY ALLOYS

A THESIS

Submitted in partial fulfillment of the
requirements for the award of the degree
of
Master of Technology

by

RHISHIKESH DARSHAN

DEPARTMENT OF METALLURGY ENGINEERING AND MATERIALS SCIENCE
INDIAN INSTITUTE OF TECHNOLOGY INDORE
JUNE, 2020

INDIAN INSTITUTE OF TECHNOLOGY INDORE

CANDIDATE'S DECLARATION

I hereby certify that the work which is being presented in the thesis entitled **MICROSTRUCTURAL EVOLUTION AND CORROSION BEHAVIOR OF FeCoNiCrVZr HIGH ENTROPY ALLOYS** in the partial fulfilment of the requirements for the award of the degree of **MASTER OF TECHNOLOGY** and submitted in the **DEPARTMENT OF METALLURGY ENGINEERING AND MATERIALS SCIENCE, Indian Institute of Technology Indore**, is an authentic record of my own work carried out during the time period from July, 2018 of joining the M.Tech. program to June, 2020of M.Tech. Thesis submission under the supervision of Dr. Mrigendra Dubey Sir, Assistant Professor, Metallurgy Engineering and Materials Scienceand Dr. Sumanta Samal Sir, Assistant Professor, Metallurgy Engineering and Materials Science.

The matter presented in this thesis has not been submitted by me for the award of any other degree of this or any other institute.

19/06/2020

Signature of the student with date
(Rhishikesh Darshan)

This is to certify that the above statement made by the candidate is correct to the best of my/our knowledge.

M. Dubey 29/06/2020

Signature of the Supervisor of

M.Tech. thesis (with date)
(Dr. Mrigendra Dubey)

S. Samal

Signature of the Supervisor of

M.Tech. thesis (with date)
(Dr. Sumanta Samal)

Rhishikesh Darshan has successfully given his/her M.Tech. Oral Examination held on **25/06/2020**.

M. Dubey 29/06/2020 S. Samal

Signature(s) of Supervisor(s) of M.Tech. thesis
Date: 29/06/2020

Convener, DPGC
Date:

M. Jayaprakash

Signature of PSPC Member
Date: 29/06/2020

Manish

Signature of PSPC Member
Date: 29/06/2020

Signature of PSPC Member
Date: 30/06/2020

ACKNOWLEDGEMENTS

It is a pleasure to thank many people who made this work possible.

First and foremost, I would like to thank my advisors, Dr. Mrigendra Dubey and Dr. Sumanta Samal whose support and guidance with pleasurable behavior have driven me to do this work. Their friendly nature gave me the freedom and opportunity to interact with them as much as I wanted to.

I would like to take this opportunity to thank my PSPC members Dr Vinod Kumar, Dr. Manish Kumar Goyal and Dr. J. P. Murugesan for their valuable time in assessing my work during the mid-term and end-term presentations and giving me valuable suggestions related to my work.

I am also thankful to the HOD MEMS and the faculty of this institution for their support and effort in teaching the concepts in Materials Science and Engineering with a highly pleasurable behaviour.

I am also thankful to my all lab mates, especially Reliance Jain and Yeeshu Sahu for their kind support.

I thank my classmates, friends and all the students and employee at the Institute for the good time I had here.

Finally, I thank my parents for their constant support.

DEDICATION

Dedicated To my Guide
My Parents
My Teachers
My Friends

Abstract

Recently, high entropy alloys (HEAs), a new class of alloys that contains five or more principal elements in equiatomic or near equiatomic proportional ratio (5-35 wt%), have attracted increasing attention because of their unique compositions, microstructures, corrosion behaviour and other adjustable properties. The configuration entropy in the HEAs tends to stabilize the solid solution formation, such as body-centred-cubic (BCC), face-centred-cubic (FCC) and/or hexagonal-closed-pack solid solution. Now, HEAs are considered as a paradigm shift for the next generation high-temperature alloys in the extreme environments, such as aerospace, cutting tools and bearing applications. In this work, microstructure evolution and corrosion behaviour of $(Fe_{25}Co_{25}Ni_{25}Cr_{20}V_5)_{100-X}Zr_X$ (x=0, 2.5, 5, 7.5, 10 at. %) HEAs were studied. The reported HEAs were cast in the high vacuum arc melting cum casting unit under the pure argon gas environment. Using a combination of scanning electron microscopy (SEM), X-ray energy spectroscopy analysis and X-ray Diffraction techniques, three phases were identified in the as-cast conditions: FCC, two mixed solid solutions phases. The microscopic results were consistent with thermodynamic simulations. The effect of Zr on microstructural evolution of HEAs is systematically investigated. The corrosion tests of FeCoNiCrV HEA were performed using potentiodynamic polarisation method in the solutions: pure H_2O, Sea Water, 3M NaCl, 3M NaOH and 3M HCl. The developed HEA shows better corrosion resistance property as compared to the conventional IS2062 steel. The results of the corrosion tests were found to be very much in cognizance with the theoretical analysis.

TABLE OF CONTENTS

LIST OF FIGURES

Figure 16: (a) SEM Image at 2000X and (b) Microscopic Image at 1600X at Zr = 7.5 at%.s

Figure 17: (a) SEM Image at 2000X and (b)Microscopic Image at 1600X at Zr = 10 at%.

Figure 18: X-Ray Diffraction Patterns HEAs at Zr = 0, 2.5, 5.0, 7.5 and 10 at%.

Figure 18a: Optical Image of $FeCoNiCrVZr_0$ HEA in 3M HCl.

Figure 18b: Optical Image Mild Steel in 1M HCl.

Figure 19: Potentiodynamic Polarization Curves for HEA at Zr = 0 at% Steel IS2062.

LIST OF TABLES

NOMENCLATURE

i	Current density (Am^{-2})
q	Charge density (Cm^{-3})
t	Time (s)
z	Number of electrons transferred (unit-less)
F	Faraday's constant (96500 C/mol)
E	Electric field intensity (NC^{-1})
σ	Conductivity ($\Omega^{-1}\ m^{-1}$)
$\emptyset$	Corrosion potential (V)
$\emptyset_0$	Free corrosion potential (V)
i_0	Free current density (Am^{-2})
CR	Corrosion rate (mm $year^{-1}$)
v	Reaction rate (mol $m^{-2}\ s^{-1}$)
ρ	Density (kg m^{-3})
M_w	Molecular weight (kg mol^{-1})
a_a	Anodic transfer coefficient (V)
a_c	Cathodic transfer coefficient (V)
α	Anodic Tafel parameter (V)
β	Cathodic Tafel parameter (V)
e^-	Electron

ACRONYMS

BCC Body centred cubic

EBSD Electron backscatter diffraction

EDX Energy-dispersive X-ray spectroscopy

FCC Face centred cubic

HEA High-entropy alloys

SEM Scanning electron microscope

XRD X-ray powder diffraction

Chapter 1

Introduction

Studies and research & developments, effortlessly, are being conducted in search of superior materials with respect to different backdrops to make the planet earth more inclusive habitable. Corrosion of materials is one of the major concerns before industrialists as it used to take a significant amount of Gross Domestic Product (GDP) of the economies. High entropy alloys (HEAs) are a new class of alloys that are now a focus of study in the fields of corrosion and metallurgy. HEAs rely on high configurational entropies because of multiple principal alloying elements, as opposed to traditional alloying where elements are alloyed with a single principal alloying element. This new alloying methodology has greatly expanded the study of new alloys due to the vast compositional space now available for study. HEAs have shown enhanced physical and chemical properties, making them of interest in a wide range of industrial uses.

Corrosion can be defined as the unintentional degradation or deterioration of material when exposed to actual environment; it is electrochemical in nature and usually begins at the surface. The metallic corrosion problem is one of the significant proportions; in economic terms, it has been calculated that approximately 5% of an industrialized nation's income is lost out on account of corrosion prevention and the maintenance or replacement of products lost or contaminated as a result of corrosion reactions. The consequences of corrosion are all very much common. Familiar live examples include the rusting of automotive body panels and radiator and exhaust components. Corrosion affects materials in a variety of industries, leading to material failure during the service life of products and equipment. The failure and replacement of current materials in service come at a great economic cost, the US alone spent $1 trillion in 2013 or

6.2% of the GDP on corrosion-related costs, while globally corrosion accounts for about 3% of the global GDP. The development of materials which are corrosion-resistant and coatings capable of extending the lifespan of equipment and structures can greatly reduce current economic expenses. Previous research of corrosion-resistant materials has been largely arrowhead on stainless steels, nickel-based alloys, as well as titanium-based alloys using conventional metallurgy, where low concentrations of beneficial alloying additions such as Cr, Mo, Ni, W, N have been used to improve the corrosion resistance of the primary alloy. The enhanced corrosion resistance of these alloys is the result of the ability of these alloying additions to generate a protective oxide layer, which prevents corrosion of the underlying surface of the metal. The enhanced corrosion resistance of these alloys has made them staples in a wide range of industries, from food and chemical production to nuclear power and waste containment.

Chapter 2

Review of Past Work and Problem Formulation

2.1 DEFINING HIGH ENTROPY ALLOYS

2.1.1 Alloy Structure

Multiple-element systems have been an area of interest since they were proposed by Yeh et al. [2]. These alloy systems have since been known as high-entropy alloys (HEA). HEAs are traditionally considered to be single-phase solid solutions composed of five or more elements at equimolar or near equimolar composition [2, 3]. However, the literature considers a wide variety of multiphase alloys as meeting the criteria for a HEA. HEAs have been of interest because they possess unique properties, for example high strength and hardness, exceptional wear-resistant properties, as well as high-temperature strength, all of which could prove to be beneficial in a variety of industrial applications. In contrast to conventional corrosion-resistant alloys, HEAs consist of many principal alloying elements. In theory, multiple principal alloying elements allow for extensive compositional freedom as well as greater property control compared to traditional primary element alloys. Due to the high entropy mixing effect [2], where the tendency of an alloy to order or segregate is greatly reduced due to the entropy of mixing, alloys composed of greater numbers of primary elements are, therefore, less likely to form ordered structures. Consequently, HEAs have a tendency to form disordered solid solutions of face-centred cubic (FCC), body-centred cubic (BCC), or hexagonal close-pack (HCP) structures [4-6], instead of more complex intermetallic phases. The locally disordered chemical environment, which results from the random arrangement of constituent elements within these

solid solutions has been theorized to lead to the unique corrosion properties of HEAs [4].

2.1.2 Corrosion Resistance

Conventional corrosion-resistant alloys, such as stainless steels, rely on the formation of a protective surface oxide layer. Therefore, HEAs with compositions similar to stainless steel or other corrosion-resistant alloys will show similar corrosion resistance and oxide formation. Stainless steels and their alloying have been studied for the past several decades due to their corrosion resistance and the nature of their passive films. Several elements, such as Cr and W, have been identified as strong oxide formers, which, when added to stainless steels, contribute to their corrosion resistance. Other elements, such as Mo and N, also improve corrosion resistance, but likely by dissolving and then altering the local pit environment. Stainless steels and other alloys have been extensively modelled by empirical methods, which have generated tools for industry design of corrosion-resistant alloys. One such tool, the pitting resistance equivalent (PRE) number (or PREN) [7-11], is described by [7]:

$$PREN = wt.\%Cr + 1.6wt.\%W + 3.3wt.\%Mo + 16wt.\%N \qquad Eq.\ (1)$$

This equation was created from large amounts of empirical data to guide the selection of stainless steel alloys for applications where stainless steels would be susceptible to localized corrosion. The knowledge of all possible alloying elements, which are key factors in the determination of an alloy's PREN, have not been studied to the same degree, leaving a large knowledge gap in the prediction of HEA corrosion resistance. HEAs possessing similar oxide-forming elements as conventional corrosion-resistant alloys such as Cr, W, etc., which are capable of oxide layer formation, may greatly reduce the corrosion rate of a material. However, HEAs, in contrast to conventional alloys, have the ability to be comprised of considerably larger compositional fractions of beneficial elements. The

properties of HEAs are considered to be closely related to the properties of their constituent elements. However, these alloys also rely on the interactions between compositional elements [12], which can play a critical role in the overall properties. Chen et al. studied the CuNiAlCoCrFeSi HEA and compared it to 304 stainless steel, which has shown that the HEA is more noble than what would be predicted from the individual elements [13]. HEAs have unique corrosion properties making them of interest for use in coatings and as possible replacements for current commercial corrosion-resistant alloys.

2.2 OVERVIEW

This chapter will pay attention on the current state of knowledge of HEA production and alloying, which affects the corrosion properties of HEAs in aqueous environments. The effects of both composition and microstructure will be critically analyzed. The corrosion resistance of HEAs in both chloride- and sulfide-rich solutions will be discussed in detail, as well as the effects of alloying of well-known beneficial elements and their effects on HEA resistance to all forms of corrosion. The current methods being used in the field to gather critical electrochemical data on the corrosion of HEAs in accelerated testing conditions will also be analyzed.

2.3 LOCALISED CORROSION OF HEAs

2.3.1 Pitting Corrosion

Passive films, their breakdown, and subsequent contribution to pit formation have been studied in detail [14, 15]. Similarly, pitting corrosion of alloys, caused by a break in the passive film, has also been studied extensively for stainless steels and other corrosion-resistant alloys. One of the major disadvantages of passive materials is their susceptibility to localized corrosion. In pitting corrosion, the passive film breaks, resulting

in a surface that is susceptible to pitting. The nature of HEA pitting is still relatively unexplored. The general methods used to study the phenomena are largely electrochemical tests consisting of potentiodynamic polarisation as well as critical pitting temperature testing. Potentiodynamic polarization allows for the determination of an alloy's pitting potential [16]. The pitting potential can be described as the potential at which a stable pit begins to grow. The nobility of this potential, along with repassivation potentials that can be obtained from cyclic polarisation experiments, have been used to describe the susceptibility of alloys to pitting corrosion. The nobility of this pitting potential represents the alloy's resistance to pitting. The nobler the pitting potential, the less likely the alloy is to undergo pitting under a specific electrolyte [15]. Pitting is known to be associated with metallographic features such as second phases particles, inclusions, and defects [17]. The resulting segregation caused by these features decreases an alloy's resistance to pitting corrosion, due to their greater susceptibility to pit initiation [18]. The temperature has been studied as a critical factor in pitting corrosion of alloys [16]. There is often a critical temperature below which an alloy will not pit, and above which pitting is observed. At temperatures below the critical pitting temperature (CPT) an alloy will undergo transpassive dissolution at high potentials, while above the CPT the alloy will be susceptible to pitting at potentials below the transpassive potential. The CPT is commonly used to describe an alloy's resistance to pitting corrosion—the higher the CPT, the greater the resistance to pitting corrosion [15, 19].

2.4 CURRENT ALLOY PROCESSING AND GENERATION

Production and processing of HEAs have largely been focused on the ability of HEAs to present desirable properties, such as making conventional alloys lighter and stronger. HEAs have been studied largely

for their enhanced properties and capability to consist of large compositional fractions of desired elements, which allow these materials to be extremely tunable [2, 20], thereby generating novel alloys with improved properties unattainable by conventional alloying and processing methods.

2.4.1 Processing of single-phase alloys

Alloying elements play a significant role in the properties and microstructures of HEAs. Not much is known in the way of designing and processing these alloys. Therefore most alloys are either left unprocessed in the as-cast condition or held at high temperatures for long periods of time in order to generate homogenized and heterogeneous phase alloys preferable for study. Li et al. [21] studied the effect of alloying elements on the microstructure of the FeNiCrCu composition by adding alloying elements Co, Al, Mo, Mn, and Zr in equiatomic mole fractions to the base composition. This study shows that these alloying additions can greatly change the microstructure and properties of the HEA. The HEAs were compared using optical microscopy, scanning electron microscopy, and x-ray diffractometry techniques. Results show that when alloy composition is comprised of elements near the III, V family group of the periodic table (i.e. FeNiCrCuCo and FeNiCrCuMn), a single-phase FCC structure is observed. When Zr is added in the case of FeNiCrCuZr HEA, the alloy system consists of BCC solid solution phase along with intermetallics. It was found that the typical nature of a HEA microstructure is a combination of dendrites and interdendritic regions throughout the microstructure. There are complex interactions present in HEA systems that create a diverse number of microstructures, which can be highly tuned to produce ideal microstructures for a variety of applications. The alloying of HEAs with Cu and Al is a primary concern when looking at the corrosion resistance of HEA. The effects of Cu alloying have been studied by Hsu et al. in the $FeCoNiCrCu_x$ HEA system in 3.5% NaCl solution

[22]. Evaluation of corrosion properties was done by both immersion and potentiodynamic polarization tests. The microstructural analysis done with SEM/EDX shows segregated interdendritic regions with high amounts of Cu. The copper segregation into these regions leads to major corrosion of the interdendritic due to galvanic coupling with the dendritic regions. The alloying of Cu and subsequent segregation leads to the poor corrosion resistance of these copper-rich HEA compositions. Al has been seen to have similar negative effects on the microstructure and phase composition of HEAs. Increased alloying of Al has been studied by Kao et al. in $Al_xCoCrFeNi$ HEA to change the microstructure from a purely FCC microstructure at low Al contents between 0 and 0.25 atomic fraction, while possessing both FCC and BCC phases when the atomic fraction of Al is greater (0.5 and 1) [23]. The change in microstructure corresponds to a sharp decline in corrosion resistance seen in various chloride-containing sulfuric acid solutions at 25ºC. A strong decrease in breakdown potential, as well as an increase in passive current density, are seen when the microstructure changes from FCC to FCC+BCC [23]. The segregation of many different elements has been seen to have detrimental effects on the corrosion resistance of HEA alloys. Currently, the HEAs that are most resilient to the effects of corrosion have been single-phase alloys. Single-phase alloys have a number of beneficial properties that make them of primary interest when generating a corrosion-resistant HEA [12, 17]. Corrosion resistance of single-phase HEAs has been largely attributed to their inclusion free, uniform solid solution nature. Subsequent work has been done to predict and generate single-phase HEAs by thermodynamic calculations, and phase predictions.

2.5 CORROSION BEHAVIOR OF HEAs

2.5.1 Corrosion resistance of HEAs in chloride solutions

The corrosion resistance of HEAs in chloride solutions has been studied to better understand the corrosion resistance behaviour of HEAs compared to conventional corrosion-resistant alloys of similar compositions. The $Co_{1.5}CrFeNi_{1.5}Ti_{0.5}Mo_{0.1}$ HEA has been studied by measuring both pitting potential (Epit) and critical pitting temperature (CPT) in 1M NaCl, and 1M NaCl + (0.1,1M) $NaNO_3$ chloride solutions [24]. The $Co_{1.5}CrFeNi_{1.5}Ti_{0.5}Mo_{0.1}$ alloy exhibits an FCC solid solution structure [23]. The effect of Cl concentration was determined by simultaneously testing Epit and CPT using potentiodynamic polarisation tests at temperatures ranging from 25 to 80ºC. Through the range of temperatures in deaerated 0.001 and 0.01M NaCl solutions, the alloy shows a very high transpassive potential, which varies very little with temperature. The alloy CPT was tested using a potentiodynamic technique in solutions of 0.1, 0.5, and 1 M NaCl with temperatures ranging from 25 to 80ºC. The potentiodynamic curves can be used to monitor CPT by observing when there is a change from transpassive dissolution, which is denoted by a gradual increase in the current, while pitting corrosion is seen by a steep decrease in breakdown potential, occurring within the conventional passive potential range. The CPT was found to depress by increase in [Cl^-]; the CPT of $Co_{1.5}CrFeNi_{1.5}Ti_{0.5}Mo_{0.1}$ was found to be 70, 60, and 60ºC for solutions 0.1, 0.5, and 1 M NaCl respectively. The influence of [Cl^-] on corrosion of HEAs has been shown to be very complex. Chou et al. reported that Leckie et al., Wang et al., and Meguid et al. have seen that pitting potential was proportional to the logarithm of the chloride concentrations at a constant temperature [24]. The result seems to be in agreement that increases in both temperature and [Cl^-] decrease the pitting resistance of the alloy [24]. Newman has attributed this effect to the increased porosity of the passive film at high temperatures allowing for the formation of chloro-complexes of chromium [25]. Chen et al. compared CuNiAlCoCrFeSi HEA and compositionally similar 304SS with near equal Cr content in deaerated 1 M NaCl solution at room temperature

[13]. The HEA was shown to be more noble and have a lower corrosion current density than 304SS in NaCl. The HEA can be described as having greater resistance to uniform corrosion, due to the nearly amorphous HEA structure, which contains little to no grain boundaries, allowing for greater congruence of the passive film. The passive region of the HEA is smaller than that of 304SS, and when the HEA passive film is ruptured, the alloy is more susceptible to nucleation and growth than 304SS.

2.5.2 Corrosion Resistance of HEAs in sulfide solutions

The corrosion resistance of HEAs in sulfide [SO_4^{2-}] solutions was studied in an identical manner to [Cl^-]. Potentiodynamic polarization measurements of $Co_{1.5}CrFeNi_{1.5}Ti_{0.5}Mo_{0.1}$ were made in solutions of 1 M NaCl containing 0.1, 0.25, 0.5, 0.75, and 1 M Na_2SO_4 in temperatures ranging from 25 to 80ºC. All potentiodynamic curves show an active-passive corrosion behaviour over the entire temperature range [13]. The pitting potential increased with the increase of [SO_4^{2-}]. The increased of [SO_4^{2-}] had a positive effect on the pitting resistance of the alloy in the solution, with the pitting potential and the CPT of the alloy being higher in the 1 M NaCl + 1 M Na_2SO_4 solution. The addition of SO_4^{2-} ions has shown to be an inhibitor of pitting corrosion. The difference between Ecorr and Epit increases with increasing SO_4^{2-} concentration, therefore it can be determined that SO_4^{2-} in Cl solutions act as a pitting inhibitor. Chen et al. tested CuNiAlCoCrFeSi HEA in H_2SO_4 and compared potentiodynamic polarisation curves to 304SS [13]. In deaerated H_2SO_4 solutions at room temperature, the HEA was shown to have a greater resistance to general corrosion than 304SS. However, the range of potentials in which the HEA remains passive is much smaller than 304SS. Pitting corrosion is not observed in either the 304SS or HEA in 1 N H_2SO_4 [13]. Therefore, it can be seen that pitting is either decreased or more often absent after accelerated testing of HEAs in sulfate-containing solutions. However, the corrosion resistance of an HEA system in sulfate is

dependent on the alloying composition. It has been seen that these HEAs have improved corrosion properties compared to the commercial alloys. HEA properties have shown to be advantageous when comparing the total alloy to the sum of its parts from an electrochemical viewpoint.

2.6 EFFECTS OF ALLOYING ON HEA CORROSION RESISTANCE

2.6.1 Effects of Cr content on HEAs

Chromium has conventionally been relied on the production of stainless steels and other corrosion-resistant alloys such as nickel-based alloys to induce the formation of a chromium oxide rich passive film. The amount of Cr alloyed in a steel is critical in ensuring stainless quality. Newman et al. prepared high purity Fe-Cr polycrystals from which 7.3, 9.4, and 10.9 wt.% plate electrodes were prepared [25]. Anodic polarisation was performed in deaerated 1 M H_2SO_4 at room temperature. Incomplete passivity was confirmed in the 10.9 wt.% Fe-Cr samples, providing sufficient evidence that a Cr concentration between 12-13% is required to be considered passive stainless steel. Lee et al. studied $AlXCrFe_{1.5}MnNi_{0.5}$ with varying Al content by potentiodynamic polarisation in 0.5 M H_2SO_4 solutions. All alloy compositions show an active-passive corrosion nature with high resistance to general corrosion at high potentials. The Al free $CrFe_{1.5}MnNi_{0.5}$ alloy demonstrated the lowest passive current density [26]. Potentiodynamic polarization in 1M NaCl at room temperature shows spontaneous passivity with higher Epit associated with lower Al concentrations. These alloys and most HEAs where chromium is a primary alloying element have chromium compositions greater than 13wt.%, which can be associated with the enhanced corrosion-resistant properties of most HEAs. However, there is still a large knowledge gap in the area of the oxide film that forms on the surface of these HEAs [26]. It is not necessarily true that a HEA high in chromium will have a

chromium-oxide surface film or if other oxides or un-oxidized element will be present in the oxide layer of any particular HEA.

2.6.2 Effects of Mo alloying

Mo has been conventionally used in corrosion-resistant alloys as it is known to assist in the repassivation of pits in acid and chloride environments [27]. However, in many HEAs Mo and Cr segregate, forming a sigma phase rich in both elements [28]. The strong metal-metal bond strength between Mo and Cr that causes this segregation can be detrimental to the overall corrosion resistance of such Mo-containing HEAs. The effect of Mo concentration has been studied by Chou et al. in a $Co_{1.5}CrFeNi_{1.5}Ti_{0.5}Mo_x$ alloy series by potentiodynamic polarisation testing in 0.5 M H_2SO_4, 1 M NaOH, 1 M NaCl. The Mo composition was varied from 0 to 19.96 wt.%. In deaerated 0.5 M H_2SO_4, all alloys presented similar corrosion resistance [28], while in 1M NaOH Mo containing alloys showed a decreased resistance to corrosion in both an increase i_{corr} and a decrease in breakdown potential. However, the Mo-containing alloys showed improved resistance to pitting in 1M NaCl. The Mo-containing alloys showed a much wider passive region as well as Epit between 1.1-1.2 V SHE, far more noble than Epit, 0.33 V SHE, of the Mo-free composition. Molybdenum has been shown to be a beneficial alloying addition, which increases an alloys resistance to pitting in Cl- rich solutions.

2.6.3 Effects of Al, Co, and Mn

The effects of Al alloying was studying by both Lee et al. [26] and Kao et al. [23] using $Al_xCoCrFeNi$ and $Al_xCrFe_{1.5}MnNi_{0.5}$ alloy series, respectively. Both alloy systems were tested potentiodynamically in 0.5 M H_2SO_4, giving a basis for comparison when substituting Co for Mn. The alloying of Al in both cases has been seen to have little to no effect on the corrosion response in sulfuric acid solutions in the Co-containing alloy.

However, the increase in Al content has a deleterious effect at higher temperatures, which can be seen in an increase in passive current density. The Mn-containing alloy increased the passive current density with the increase of Al. Both compositions show a negative effect on corrosion resistance, which corresponds to the addition of Al. The replacement of Co with Mn in the Al-free CoCrFeNi alloy weakens the corrosion resistance of the alloy in the corresponding 0.5 M H_2SO_4 solution. The resistance of the MnCrFeNi alloy is lower than common 304SS. The effect of Al alloying is closely related to the formation of a multiphase FCC-BCC alloy, which corresponds to a reduction in corrosion resistance of the alloys.

2.6.4 Effects of Ni alloying

In the stainless steel industry, nickel has conventionally been used as an austenite phase stabilizer. Ni-Mo and Ni-Cr alloy systems have shown to be highly resistant to corrosion in acidic solutions, both sulfuric and hydrochloric acids. The alloying effect of Ni on the corrosion resistance of HEAs has been studied by Qiu et al., by potentiodynamic polarisation testing of the $A_{l2}CrFeCoCuTiNi_x$ series, x ranging as 0, 0.5, 1, 1.5 and 2, in 3.5wt. % NaCl and 1 M NaOH. The alloy of high corrosion resistance was seen to be a molar ratio of 1, suggesting that there is a critical content of Ni at which point if the Ni content is increased there are detrimental impacts on the corrosion resistance [29]. The microstructures of alloys containing a greater concentration of Ni were seen to form a detrimental Al, Ni-rich B2 phase, which may negatively affect the corrosion resistance of the alloy studied. The Ni alloy composition and its effects on corrosion resistance are still relatively unknown.

Chapter 3

Methodology

FOUR CORE EFFECTS OF HEAs

There are multiple factors that can affect the microstructure and properties of HEAs. Among these factors, four core effects are most important and basic (Yeh, 2013a). Because HEAs consist of atleast five principal elements, and conventional alloys are based on one or two metallic elements, many different basic effects exist between these two class of materials. The four core effects are: high entropy, severe lattice distortion, sluggish diffusion, and cocktail effects (Yeh, 2006, 2013a). Thermodynamically, the high-entropy effect could interfere with complex phase formation. In terms of kinetics, sluggish diffusion effect could limit down the speed of phase transformation. In structure, severe lattice distortion effect could deviate properties to an extent. In properties, a cocktail effect brings excess to the quantities predicted by the mixture rule due to mutual interactions of unlike atoms and severe lattice distortion.

3.1 High-Entropy Effect

The high-entropy effect is the most prima facie effect because it can drive forward the formation of solid solutions and enables the microstructure much easier than expected. High entropy effect provides support in the formation of a simpler solid solution in HEAs rather than the formation of various intermetallics, especially at greater temperatures. The high entropy effect creates enabler environment that support the formation of a disordered solid solution rather than ordered intermetallics. Elemental phases have small negative ΔH_{mix} and ΔS_{mix} as they are based on one principal element. Compound phases have great negative ΔH_{mix} but low

ΔS_{mix} because ordered structures have low configurational entropy. But random solid solution phases containing multi-components have middle range negative ΔH_{mix} and highest ΔS_{mix}.

The Gibbs free energy of mixing, ΔG_{mix}, is given by

$$\Delta G_{mix} = \Delta H_{mix} - T\Delta S_{mix}$$

where ΔH_{mix}: enthalpy of mixing and ΔS_{mix}: entropy of mixing, a higher number of element would potentially reduce the mixing free energy, especially at elevated temperatures by contributing larger ΔS_{mix}. Therefore, a disordered solid solution phase is more stable at elevated temperature than ordered intermetallic phases. It enhances the formation of a solid solution phase due to which solution hardening takes place in solution phase, causing a rise in the strength and ductility of HEAs. The stronger bond energies will grade up the formation of a solid solution rather than intermetallics compound.

3.2 Severe Lattice Distortion Effect

It is important to note that due to multi-component matrix of different solid solution phases in HEAs, each atom is surrounded by a different kind of atom thus causing severe lattice strain and stress due to the atomic size difference.

Along with different atomic size difference, different bonding energy and crystal structure of consisting elements also leads to higher lattice strain. Lattice distortion not only affects various properties but also reduces the thermal effect on properties. Lattice distortion causes significant electronic scattering leading to a decrease in electrical conductivity of HEAs. Phonon scattering is also large in HEAs due to severe lattice distortion leading to a decrease in the thermal conductivity.

Lattice distortion caused by thermal vibration is less than the severe lattice distortion in HEAs causing it insensitive towards the change of temperature.

3.3 Sluggish Diffusion Effect

HEAs consist of random solid solution phases along with the ordered solid solution, causing sluggish diffusion of atoms and vacancies leading to the chemical stability of the HEAs. A vacancy in the whole matrix of solute is in fact surrounded and competed by different-element atoms during diffusion. It has been proposed that slower diffusion and higher activation energy would occur in HEAs due to greater fluctuation of lattice potential energy (LPE) between lattice sites. These abundant available low-LPE sites can act as traps and provide hindrance to the diffusion of atoms. This arrowheads to the sluggish diffusion effect.

It is expected that sluggish diffusion might affect phase nucleation, growth and distribution, and morphology of a new phase through diffusion-controlled phase transformation.

Sluggish diffusion helps in improving the properties and microstructure of the HEAs. As sluggish diffusion leads to finer grain structure causing good toughness and strength. It also improves the creep property causing prolong life at high temperature.

3.4 Cocktail Effect

This term is coined by Prof. Ranganathan to study the properties that get enhanced in HEAs[. The enhancement of properties of HEAs may be due

to the interaction of different properties of different constituent phases present in HEAs. Generally, mixture rule is used to calculate the value of properties in conventional alloy system, but when the same rule is applied in HEAs. There is a severe difference in the experimental value and value obtained from the mixture rule. This variation in property of HEAs arises not only due to basic properties of elements by the mixture rule but also from the mutual interactions among all the elements and from the severe lattice distortion. Mutual interaction and Lattice distortion also lead to great change in the quantified values of the properties in case of HEAs. The cocktail effect brings many positive effects in HEAs such as high magnetization, low coercivity, good plasticity, high strength, and high electrical resistance.

Chapter 4

Experimental

The HEA systems consisting of Fe, Co, Ni, Cr, V and Zr were synthesized based on chemical formula $(Fe_{25}Co_{25}Ni_{25}Cr_{20}V_5)_{100-X}Zr_X$ where x=0.0, 2.5, 5.0, 7.5 and 10.0 . The given below table is showing the details regarding compositions.

Table 1: Composition of HEAs

Constituent	At% Wt%	At% Wt%	At% Wt%	At% Wt%	At% Wt%
Fe	25.0 24.79	24.375 23.800	23.750 22.840	23.125 21.910	22.500 21.010
Co	25.0 26.16	24.375 25.120	23.750 24.110	23.125 23.130	22.500 22.170
Ni	25.0 26.06	24.375 25.020	23.750 24.010	23.125 23.030	22.500 22.080
Cr	20.0 18.47	19.500 17.730	19.000 17.020	18.500 16.320	18.000 15.650
V	5.00 4.52	4.875 4.340	4.750 4.170	4.625 4.000	4.500 3.830
Zr	0.00 0.00	2.500 3.990	5.000 7.860	7.500 11.610	10.000 15.250

4.1 Synthesis

There are three routes to synthesize the samples, but here the HEAs have been synthesized in high vacuum arc melting cum casting unit.

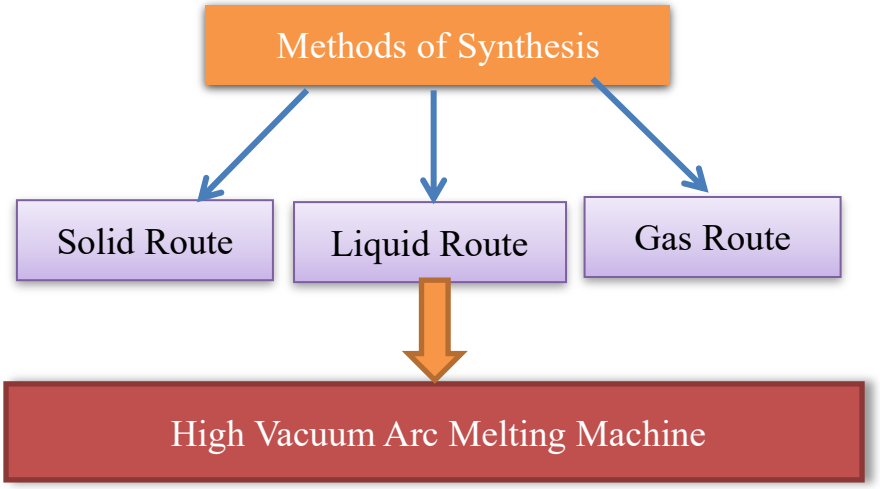

The HEAs based on chemical formula $(Fe_{25}Co_{25}Ni_{25}Cr_{20}V_5)_{100-X}Zr_X$ were synthesized in the high vacuum arc melting cum casting unit in the shape of buttons with 20g weight each and disc with 500g weight each.

WHAT IS ARC MELTING?

Arc Melting is used for melting metals usually to produce alloys. The heat is generated through an electric arc struck between a tungsten electrode and metals placed in a crucible in the copper hearth. In vacuum arc melting the chamber is evacuated and then backfilled with argon gas. Hence, the whole melting process is performed in the atmosphere of argon gas.

PRINCIPLE USED:

Basic Principle: A standard tungsten inert gas (TIG) welding unit is used as a power source. The heat generated through the electric arc struck between the electrode and the metals facilitate melting of the metals kept in the crucible to produce an alloy. The melting process is repeated to improve the homogeneity of the alloy. The created vacuum inside the chamber avoids oxidation of the melt (Ar being an inert gas does not react with molten metal).

WHAT ARE THE FEATURES?

Features: The metals inside the chamber can be heated to a temperature even above 2000ºC. A batch of nine alloys can be produce in a single evacuation, as there are nine button shaped crucibles in the hearth. About 20g of metals can be melted in these crucibles.With the use of disc shaped copper crucible, the disc of HEAs can be produced inside the chamber. There are three main parts to the high vacuum arc melting cum casting unit: power source (TIG Welding unit), chiller and vacuum unit. The vacuum unit with rotary and diffusion pumps can attain a vacuum of 10^{-6} m bar. The cold water circulated from the chiller and cools both the copper hearth and the electrodes. After elemental metals (or master alloy) are melted and solidified inside the chamber it can be 'turned over' by a 'tweezer mechanism' without breaking the vacuum (and then re-melted). The melting → solidification → 'turn over' of sample → re-melting process is typically repeated five times to achieve a better compositional homogeneity. Apart from the above mentioned hearth with nine crucibles, an additional hearth has been provided with one crucible, which can suction cast the molten alloy, in the form of thin cylinders (typically 6mm diameter).

WHERE IT CAN BE USED?

Applications:

(i) Melt elements to produce an alloy using a high-temperature arc.

(ii) Remelt alloys to improve homogeneity.

(iii) Suction cast the melt in a copper mould.

NECESSARY PARTS THAT COMPLETE IT

TURBO GAUSE

It is an essential piece of instrumentation that indicates the amount of air entering the combustion chamber. Air indication is measured as air pressure. The pressure of the passing air places pressures on the tube. The tube's internal pressure raise and the deflection in turbo gauge are accomplished.

ELECTRODE HOLDER

Electrode holder commonly known as a stinger, is a comparing device for holding the electrode securely in any position, the welding cable attaches to the holder in the hollow insulated handle. The design of the electrode holder permits quick and easy electrode exchange.

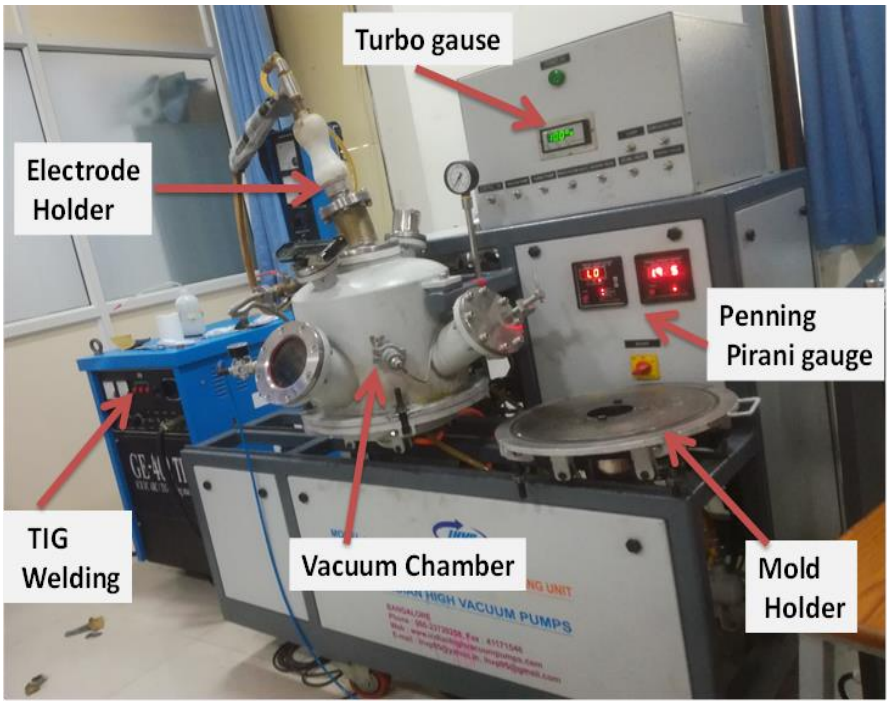

Vacuum arc melting cum casting unit

Figure 1: High Vacuum Arc Melting cum Casting

TIG WELDING

TIG electrode is made up of tungsten, which happened to be of different size and it works by simply melting the metals together without any failure. The tungsten electrode used to be shielded by a gas nozzle in order to use shielding gas more effectively. Argon is the most common inert gas used as shielding gas but in some cases helium is also used.

VACUUM CHAMBER

A vacuum chamber is a rigid enclosure made up metals from which air and other gases are removed by a vacuum pump. A produced vacuum environment facilitate the researcher to conduct physical experiments or to test mechanical devices which must operate in the actual environment.

PENNING PIRANI GAUGE

The function of Penning pirani gauge is to measures low vacuum. In the system, tungsten filament is heated up by passing a current through them.

As gas molecules interact with the filament, heat is carried away in the electrical resistance.

Synthesis of Buttons

The weighed samples of considered compositions ($(Fe_{25}Co_{25}Ni_{25}Cr_{20}V_5)_{100-X}Zr_X$, x= 0%, 2.5%, 5.0%, 7.5% and 10%) were put into button molding made up of Cu. The moulding was made up of Cu due to its high thermal conductivity and heat transfer coefficient with water. Here water works as a working fluid to transfer heat during melting operation. The mould then tightened with vacuum chamber which had tungsten rod as an electrode to generate arc in the chamber with the help of TIG welding unit.

The generated arc melted the considered samples in their respective button-shaped cavities of the moulding plate. Once the melting got completed, the button-shaped samples were taken outside the chamber after proper cooling the chamber. Now, the vacuum chamber moulding plate was cleaned properly with ethanol.

The whole process described above was repeated for 4-5 times to make the buttons homogeneous. Finally, the homogeneously formed buttons were taken outside the chamber to characterize them and to make discs for further experiments.

Figure 2: Cu Mold to cast the buttons and cast out buttons

Synthesis of Disc

After Characterization was done, three samples of compositions corresponding to Zr = 0%, 5% and 10% were selected for making pancake (discs) to perform corrosion tests on them. Now, 18 buttons for every three compositions were synthesized in the high vacuum arc melting cum casting unit in the same way as the buttons were for the Characterization. From these three groups of 18 buttons, 3 pancakes were produced in the high vacuum arc melting cum casting unit using pancake Cu moulding plate as shown in below figure.

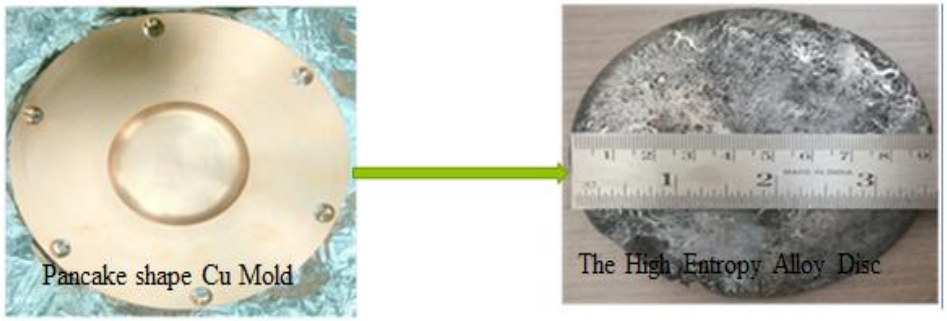

Figure 3: Cu mold to cast Pancake and Cast out Pancake

4.2 Sample Preparation

4.2.1 For Characterization

Initially, the five synthesized buttons of considered five compositions were taken to prepare samples for Characterization. These buttons were cut into almost half through Wire Electric Discharge Machine (Wire-EDM). Now, these halved buttons were grounded with different grades sand papers ranging from 240 to 2000. Finally, these grounded samples were etched in acidic solutions to perform Characterization on them.

Figure 4: Prepared samples of HEAs to observe microstructures

4.2.2 For Corrosion Test

The discs were cut into 2.5cmX2.5cm square-shaped samples with a thickness of approximately 2mm by using Wire-EDM. Now, these square-shaped samples were grounded with different grades sand papers size ranging from 240 to 2000, and then the samples were grounded with Aluminum-powders of particle size ranging from 6 micrometres to 1 micrometre. Finally, these Aluminum grounded samples were taken to perform the corrosion tests in various environment. The given below figure is showing the final grounded samples.

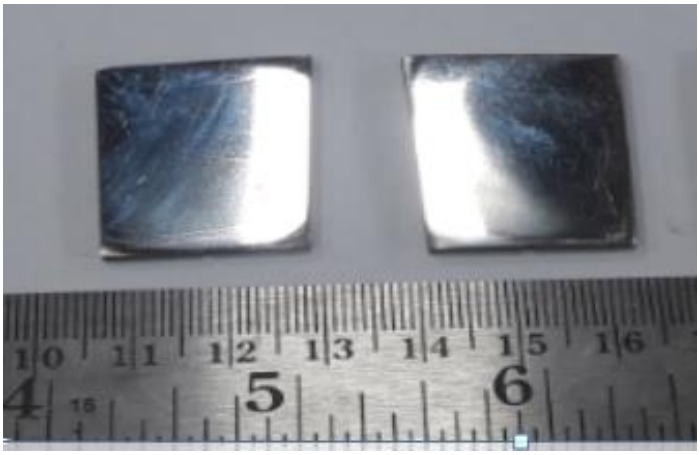

Figure 5a: The Polished samples HEA at Zr = 0 at% to perform corrosion

4.3 Characterization

4.3.1 Optical Microscope

When light enters into the eyepiece lens, it generally magnifies the image as it forms the case of an object lies in between focus and pole, so it form converge image at the first focus and this image formed by eyepiece lens act as a virtual object for the objective lens nearby it.

Again it works as the image lies between focus and pole,again it is the cases in which the image is highly magnified, virtually erect image and obtained on the screen. In this way the optical microscope works at the magnification formula:

Magnification = visual angle formed by final image /visual angle formed by object kept at D

Where D=25cm

4.3.2 Scanning Electron Microscope

Stream of electrons (primary electrons) are generated in the electron gun, and these primary generated electrons are accelerated by the grid and anode.

These accelerated primary electrons are guided to be incident on the considered sample through condensing lens and scanning coil.

When these high-speed primary electrons fall over the sample they generate low energy electrons called as secondary electrons. The collection of these secondary electrons are very difficult, and therefore, a high voltage is applied to the collector.

Now, these collected electrons generate scintillations on to the photomultiplier tube which get converted into electrical signals. These signals are amplified by the video amplifier and are fed to CRO.

By similar procedure, the electrons beams scans from left to right, and the whole picture of the sample is obtained in the CRO screen

4.3.3 Energy Dispersive Spectroscopy

Energy-dispersive X-ray spectroscopy is a chemical microanalysis technique used in couple with scanning electron microscopy (SEM). The electron vacancies are created and filled by electrons from a higher state and in result x-ray is emitted to balance the energy difference between the lower and higher energy states.

4.3.4 X-Ray Diffraction

X-ray crystallography is the experimental science that used in determining the atomic and molecular structure of a crystal.

X-ray diffraction is a non-destructive technique that used to exhibit detailed information about the crystallographic structure, chemical composition, and physical properties of materials.

The scattering of x-ray photons by atoms in a periodic lattice is elastic in nature. The scattered monochromatic x-rays having same phase result in constructive interference.

4.4 Corrosion Experiment

4.4.1Electrolytic Solutions to Perform Corrosion

Following electrolytic solutions were used in performing electrochemical corrosion experiments: Water, 3M NaCl, 3M NaOH, 3M HCl

Figure 5b: $FeCoNiCrVZr_0$ HEA samples in 3M of HCl, NaCl and NaOH kept to stabilize for 20 days

4.4.2 Electrochemical Set-Up (Electrochemical Workstation)

The schematic representation of electrochemical workstation is given that includes the following parts.

Electrochemical Cell

An electrochemical cell is a device that can produce electrical energy from the chemical reactions happening within it, or use the electrical energy reached to it to enable chemical reactions to make them happened within it. These devices possess capability of converting chemical energy into electrical energy and vice-versa. For example a standard 1.5 volt cell is the most common electrochemical cell which is used to power many electrical appliances such as TV remotes and clocks.

Working Electrode

The working electrode represents the most important component of an electrochemical cell.

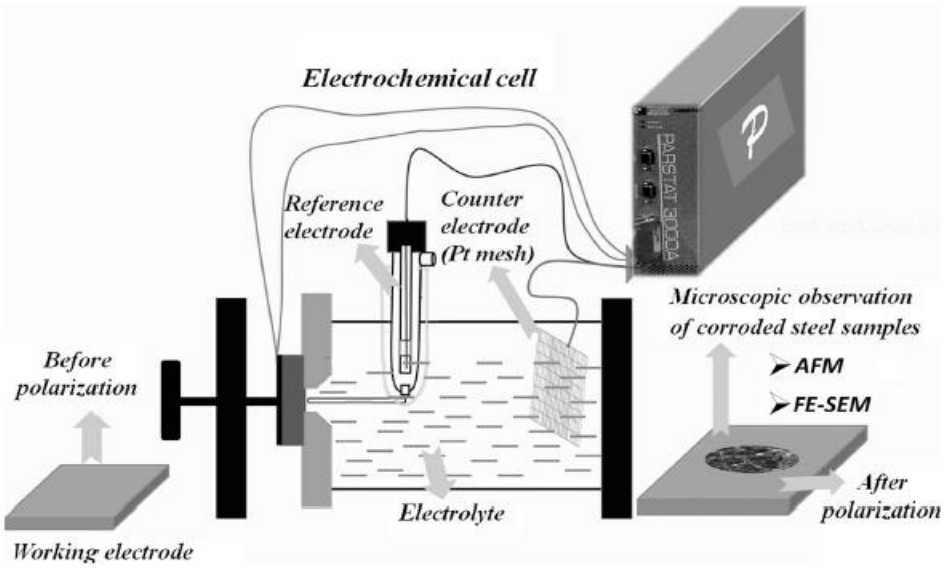

Figure 6 **:** Schematic Representation of Electrochemical Set Setup

Figure 7**:** CHI604E Potentiodynamic Polarizing Electrochemical Corrosion Setup Setup

The polished samples were washed into acetone properly to clean it from any dirt. The washed samples, then, dipped in electrolytic solutions (water, 3M NaCl, 3M NaOH and 3M HCl) and kept in the solutions for 20

days to make it make them stable with the solutions. After stabilization, the samples were taken out from these solutions and corrosion experiments were performed in the solutions in a potentiodynamic polarisation electrochemical corrosion setup.

Chapter 5

Results and Discussion

Thermodynamics parameter for HEAs:

Physicochemical and thermodynamic properties give the guideline for the prediction of phases and stability of phases in HEAs. Various parameter considered for phase stability in HEAs are mixing of entropy (ΔS_{mix}), mixing of enthalpy (ΔH_{mix}), atomic size difference (δ), valence electron concentration (VEC), and electronegativity difference [1][2][3]. All the above parameters can be calculated as follows:

$$\Delta H_{mix} = \sum_{i=1, i\neq j}^{n} \Omega_{ij} c_i c_j ; \left(\Omega_{ij} = 4\Delta H_{ij}^{mix}\right) \quad \ldots\ldots\ldots\ldots\ldots\ldots\ldots\ldots (1)$$

$$\Delta S_{mix} = -R\sum_{i=1}^{n}(c_i \ln c_i) \ldots\ldots\ldots\ldots\ldots\ldots\ldots\ldots\ldots\ldots .. (2)$$

$$VEC = \sum_{i=1}^{n} c_i (VEC)_i \quad \ldots\ldots\ldots\ldots\ldots\ldots\ldots\ldots\ldots\ldots (3)$$

$$\delta = \sqrt{\sum_{i=1}^{n} c_i \left(1 - \frac{r_i}{\bar{r}}\right)^2} ; \bar{r} = \sum_{i=1}^{n} c_i r_i \ldots\ldots\ldots\ldots\ldots\ldots\ldots\ldots (4)$$

$$\Delta\chi = \sqrt{\sum_{i=1}^{n} c_i \left(\chi_i - \bar{\chi}\right)^2} ; \bar{\chi} = \sum_{i=1}^{n} c_i \chi_i \ldots\ldots\ldots\ldots\ldots\ldots (5)$$

Where, $\Delta H_{AB}\ mix$ = Enthalpy of Mixing of binary liquid alloy AB,

C_i = Concentration of i^{th} element, r_i is the radius of the i^{th} element and $\bar{r}$ is the mean radius,

$(VEC)_i$ is the valence electron concentration of the i^{th} element.

All the above parameters for $FeCoNiCrVZr_x$ HEAs were calculated and given in table 2. It is to be noted that the mixing of entropy (ΔS_{mix}) and mixing of enthalpy (ΔH_{mix}) increases with the increase of the Zr concentration. The increase in ΔH_{mix} will lead to the formation of intermetallic compounds, while an increase in the value of (ΔS_{mix}) will lead to the formation of disorder solid solution phases. Further, VEC confirms the structure of solid solution phase(s) formed in the HEAs. FCC solid solution forms if VEC $\geq$ 8, BCC solid solution form if VEC < 6.87, and both FCC and BCC solid solution phase coexist for VEC 6.87 $\leq$ VEC < 8.0. In the present studied HEAs system; the value of (ΔH_{mix}) and VEC lie in the range -5.18 kJ/mol to -15.68 kJ/mol and 7.78 to 8.2 respectively, which indicates the possibility of formation of dual-phase microstructure. It is noticed that the entropy of mixing increases with Zr concentration, and the calculated mixing of entropy for different HEAs is in the range of 1.51R to 1.68R. The electronegativity difference is a Hume-Rothery parameter that is generally used to predict the formation of intermetallic in the HEAs. Apart from these above parameters; two others parameters are also taken into consideration to understand the phase formation.The first one is Scald ratio (Ω, the combined effect of ΔH_{mix} and ΔS_{mix}) and another is Hume-Rothery thermodynamics parameter ʌ (to understand the combined effect of ΔS_{mix} and δ), which are formulated as [2][3]:

$$\Omega = \frac{(T_m)\,\Delta S_{mix}}{\Delta H_{mix}} \quad \text{.....(6)}$$

; where Ω is a derived thermodynamic parameter known as Scald ratio

1. If the Ω > 1, shows the formation of a solid solution phase in the HEA, because of more contribution of $(T_m)\,\Delta S_{mix}$ than the (ΔH_{mix}).

2. If the Ω = 1, it is used as a critical value to understand the behaviour of the formation of a solid solution.

3. If the $\Omega \leq 1$, it shows intermetallic and segregations before the formation of a solid solution phase in the HEA. Therefore Ω values are used to estimate the formation of a solid solution phase.

$$\Lambda = \frac{\Delta Smix}{\delta^2} \quad \text{.....(7)}$$

Parameter Λ is useful to understand the phase formation and volume fraction in HEAs. If the value of Λ – Parameter is greater than equal 2.3403, it leads to the formation of a single-phase, and if it is between the ranges 0.3165 to 0.5425, it shows solid solution phase mixture. If Λ – Parameter has values less than equal to 0.2567, it shows the solid solution and intermetallic. All parameters calculated for study of $FeCoNiCrVZr_x$ (x= 0, 2.5, 5, 7.5, 10 atomic %) HEAs are given in Table 2.

Table 2: Thermo-physical properties ΔS_{mix}, ΔH_{mix}, VEC, δ%, Δχ, Ω and Λ for $FeCoNiCrVZr_x$ (X=0, 2.5, 5, 7.5, 10 atomic %)

$FeCoNiCrVZr_x$ (atomic %)	**ΔH_{mix} (KJ/mol)**	**ΔS_{mix} (J/k-mol)**	**VEC**	**δ%**	**Δχ**	**Ω**	**Λ**
X=0 %	5.18	1.51R	8.2	1.2	0.27	3.612	8.7
X=2.5%	7.98	1.59R	8.1	4.5	0.54	3.11	0.65
X=5%	10.63	1.63R	7.99	6.2	0.60	2.403	0.35
X=7.5%	13.13	1.66R	7.88	7.3	0.52	1.987	0.25
X=10%	15.48	1.68R	7.78	8.3	0.51	1.712	0.20

From the above Table 2 it is clear that the value of Scald ratio is maintained above 1 and is decreasing continuously when the concentration of Zr is increased from 0 at% to 10 at%. The Scald ratio greater than 1 indicates that the possibility of formation of a solid solution phase increases because of more contribution of $(T_m)\ \Delta S_{mix}$ than the (ΔH_{mix}), while continuously falling value of Scald ratio is exhibiting that

contribution of factor $(T_m)\,\Delta S_{mix}$ is reducing and factor (ΔH_{mix}) is rising in the formation of a solid solution in the HEAs.

In the above table 2 the parameter Λ is found to be decreasing continuously from 8.7185 to 0.2027, giving the idea about phase formation and volume fraction in the $FeCoNiCrVZr_x$ HEAs. For Zr = 0at%, the value of Λ= 8.7185 which is greater than 2.3403; directing the formation of single-phase solid solution in the $FeCoNiCrVZr_0$, the value of Λ for HEA (Zr= 2.5 at%) is 0.6528 which is less than 2.3403 but greater than 0.5425 revealing that the phase of the HEA is started to have a mixture of solid solution phases. While the $FeCoNiCrVZr_x$ HEAs with X = 5.0 at% & 7.5 atomic %, have the value of parameter Λ in the range of 0.3165 to 0.5425 exhibiting that these two HEAs have solid solution phase mixture. Finally, the value of parameter Λ =0.2027 for $FeCoNiCrVZr_x$ HEA with X = 10 at%, which is less than 0.2567 showing the HEA is a mixture of solid solution phase and intermetallics.

Thermodynamics simulation:

Thermodynamics simulation is done to predict the phases formed in the HEAs during the solidification. Thermodynamics simulation based on CALculation of PHAse Diagrams (CALPHAD) approach is used. In that approach, various thermodynamic functions such as Gibbs energy (G), Helmholtz energy (A) etc. are used to evaluate different phases that may form [4]. Thermodynamics simulation has been carried out using the ThermoCalc® software (thermo-Calc Software, Salona, Sweden) in conjunction with TCHEA2® database for $FeCoNiCrVZr_x$ (x= 0, 2.5, 5, 7.5, 10 atomic %) HEAs. Figure 8(a) and Figure 8(b) shows the phase fraction with temperature and Scheil's solidification plot for x= 0 atomic % respectively, which suggest that primary FCC_L12 phase form from the liquid, followed by the formation of a dual-phase mixture of FCC_L12 and BCC_B2 phases from the remaining liquid. It is also to be noted that for x=0 atomic %, FCC_L12, BCC_B2, SIGMA, FCC_L12#2, and

BCC_B2#2 phases are evolved during the various phase transformation. Figure 9 (a) shows the solidification pathway for x=2.5 atomic %, which indicates that the formation of primary FCC_L12 phase from liquid then followed by the formation of a dual-phase mixture (FCC_L12 + NI7ZR2) then the evolution of three-phase mixture (FCC_L12 + NI7ZR2+ C15_Laves phase). It is to be noted that for x= 2.5 atomic % and for x= 5 atomic %, FCC_L12, NI7ZR2, BCC_B2, SIGMA, FCC_L12#2, NI5ZR, CO3VV and BCC_B2#2 phases are evolved during the different phase transformation **(**given in Figure 9 (b) and Figure 10 (b)).

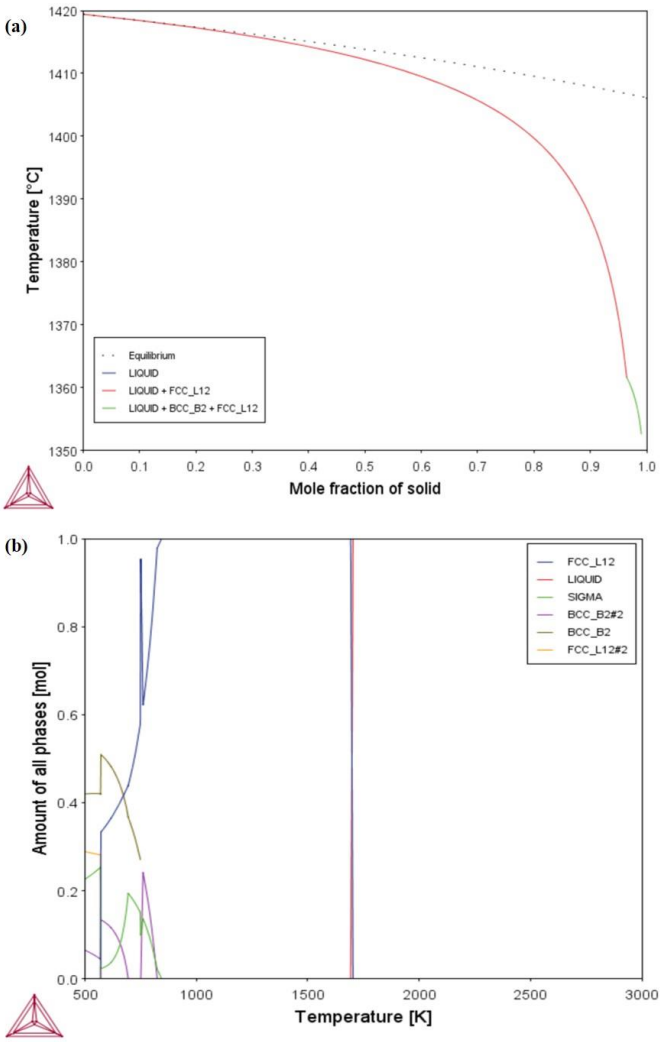

Figure. 8- (a) Mole fraction of phases with temperature plot for alloy x= 0 atomic %, (b) Scheil's solidification pathway for x= 0 atomic %.

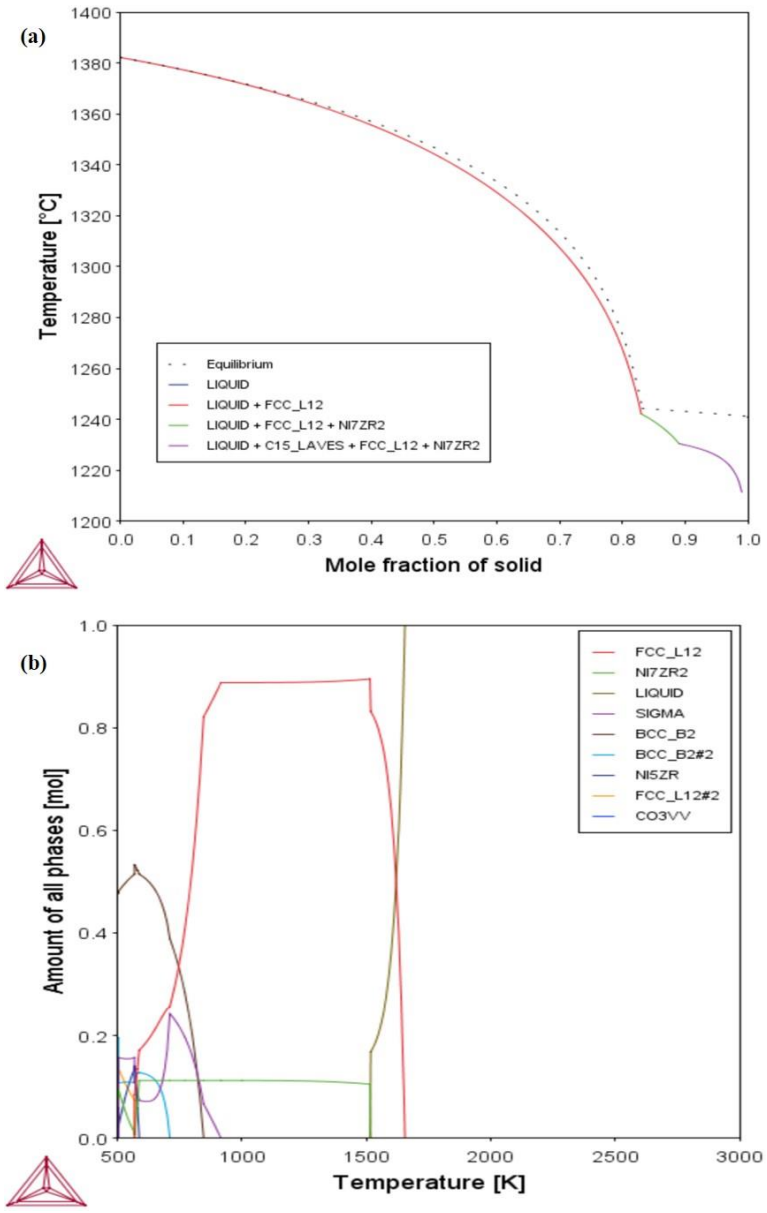

Figure. 9- (a) Mole fraction of phases with temperature plot for alloy x=2.5 atomic %, (b) Scheil's solidification pathway for x= 2.5atomic %.

Figure 10 (a) and Figure. 11 (a) show the solidification pathways for X=5 % and X=7.5 % respectively, and results show the formation of FCC_L12

from liquid then dual-phase mixture between FCC_L12 and C15_Laves phase then evolution three-phase mixture (C15_Laves phase + FCC_L12 + NI7ZR2). For x= 7.5 atomic %, FCC_L12, NI7ZR2, BCC_B2, SIGMA, and BCC_B2#2 phases are evolved during the liquid-solid and solid-solid phase transformation (given in Figure. 11 (b)).

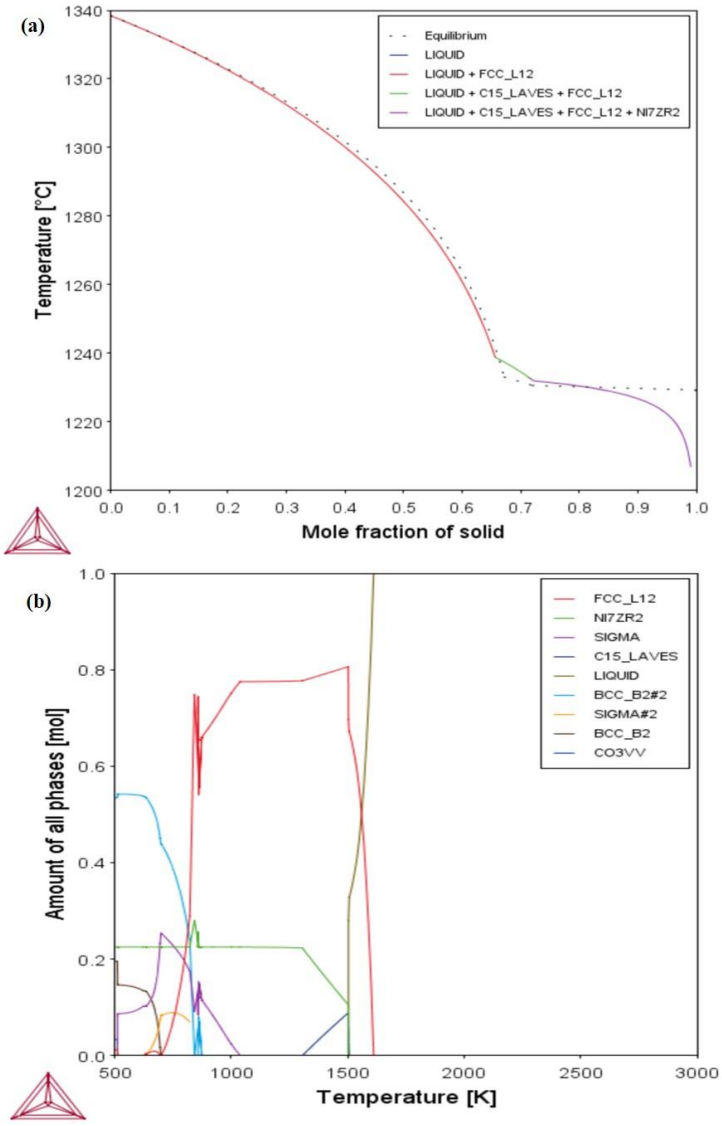

Figure. 10- (a) Mole fraction of phases with temperature plot for alloy x=5 atomic %, (b) Scheil's solidification pathway for x=5 atomic %.

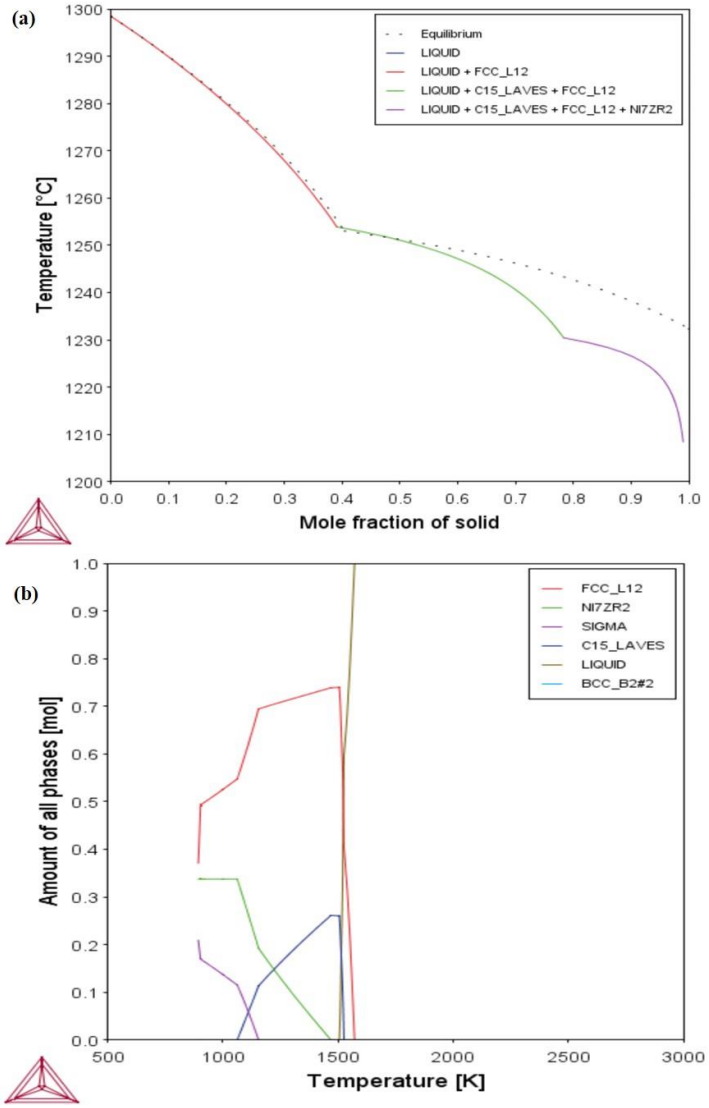

Figure. 11- (a) Mole fraction of phases with temperature plot for alloy x=7.5 atomic %, (b) Scheil's solidification pathway for x=7.5 atomic %.

Figure. 12 (a) shows the solidification pathways for x= 10 atomic % which shows the formation of primary C15_Laves phase from the liquid then dual-phase mixture between the C15_Laves phase and FCC_L12 phase then three-phase mixture (C15_Laves phase + FCC_L12 + NI7ZR2). For x= 10 atomic %, FCC_L12, NI7ZR2, BCC_B2, SIGMA, and BCC_B2#2 phases are evolved during the different liquid-solid and solid-solid phase transformation (given in Figure. 12 (b)). Further, the solidification plot we can point out that for x= 0 atomic % FCC_L12 phase dominant (more than

0.9-mole fraction) and BCC_B2 phase with a minor amount, while for others composition both FCC_L12 and C15_Laves phases present with different mole fraction.

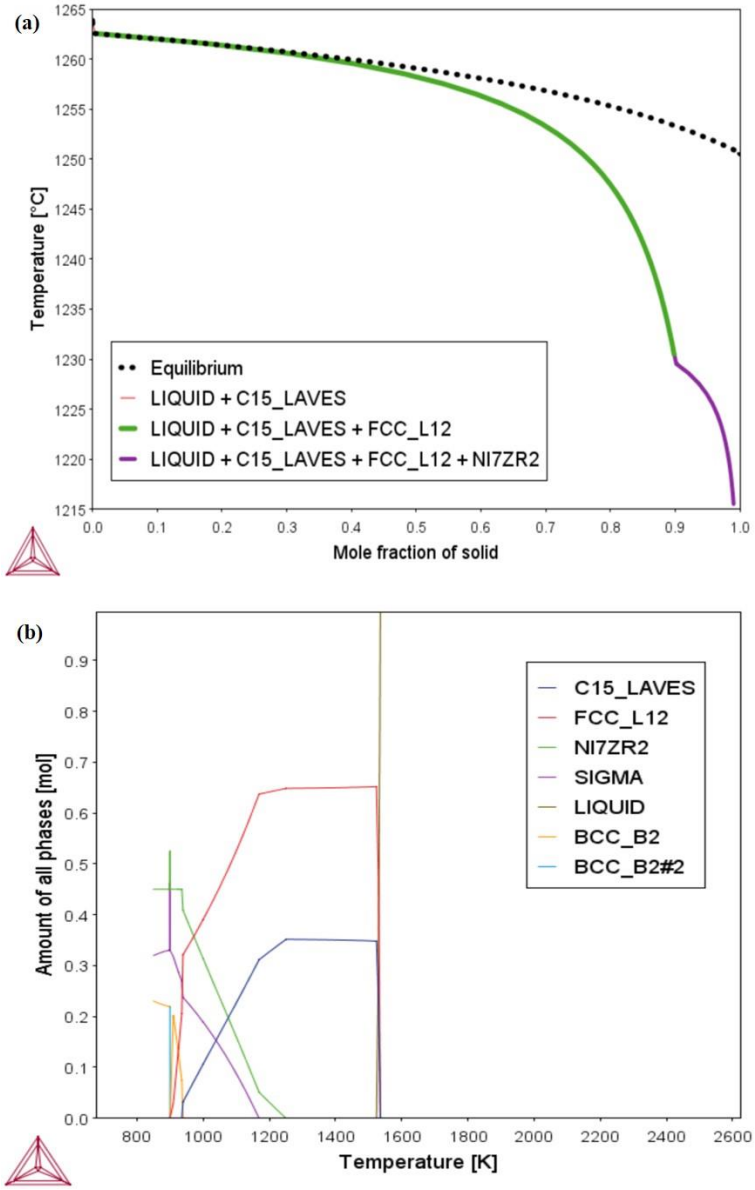

Figure. 12- (a) Mole fraction of phases with temperature plot for alloy x=10 atomic %, (b) Scheil's solidification pathway for x= 10 atomic %.

5.1Microstructural Characterization

Thermodynamically, the equilibrium state and the corresponding microstructures of HEAs result from the stability competition among all the phases in a multi-component system. HEAs in the as-cast condition generally have less number of phases than the those in the heat-treated condition, because the former almost are still in metastable or nonequilibrium state. In order to recognize the relationship between nonequilibrium and equilibrium phases in HEAs, an effective way is needed to determine and/or predict the multi-component phase diagrams. Traditionally, binary and ternary phase diagrams have been established purely through experimental methods. For multi-component systems, a phenomenological method, called Computer Coupling of Phase Diagrams and Thermochemistry (CALPHAD), has been widely applied for the study. Through this thermodynamic method, not only the known thermodynamic properties can be determined, but also the unknown thermodynamic properties can be predicted. The application of the CALPHAD approach in aiding materials design has been widely discussed and especially recently, successfully used in the AlCoCrFeNi HEAs systems by Zhang et al.

5.1.1Energy Dispersive Spectroscopy

Table 3: Energy Dispersive Spectroscopy Composition Table

Compositions	**Fe (at %)**	**Co (at %)**	**Ni (at %)**	**Cr (at %)**	**V (at %)**	**Zr (at %)**
Theoretical	25.0	25	25	20	5	0
Theoretical Actual	24.375 24.3±0.18	24.375 24±0.19	24.375 22.9±0.19	19.500 19.6±0.19	4.875 4.8±0.11	2.500 1.9±0.11
Theoretical Actual	23.750 25 ±0.20	23.750 24.1±0.19	23.750 21.6±0.19	19.000 20.5±0.11	4.750 4.8±0.11	5.000 3.4±.075
Theoretical Actual	23.125 24.9±0.18	23.125 23.1±0.19	23.125 20.8±0.19	18.500 19.3±0.11	4.625 4.9±0.11	7.500 6.8±0.11
Theoretical Actual	22.5 23.8±0.20	22.500 20.6±0.17	22.500 20.7±0.17	18.000 20.8±0.11	4.500 5±0.11	10.000 8.3±0.10

5.1.2 Optical Microscopy and Scanning Electron Microscopy

Zr=0%

The HEA sample at Zr=0% was observed under a scanning electron microscope (SEM) in a backscattered mode which has been shown in the following given figure. This SEM image is clearly revealing that the microstructure of the taken sample is a single-phase, i.e. FeCoNiCr-rich (FCC) solid solution phase.

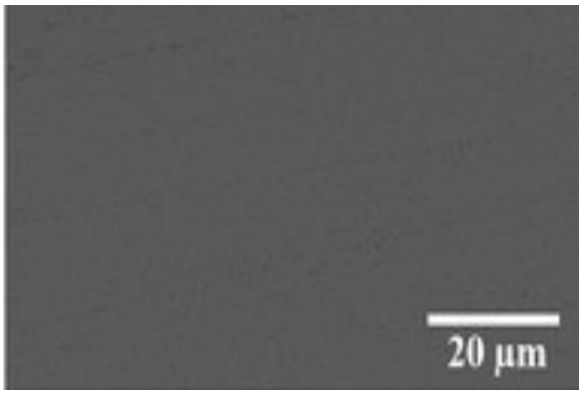

Figure 13**:** SEM Image of HEA at Zr = 0 at%

Zr=2.5%

When 2.5 at% of Zr was added to the Fe-Co-Ni-Cr-V HEA, and the prepared sample was observed under a scanning electron microscope in a backscattered mode which has been shown in the below-given figure is clearly revealing that the previously observed single phase is turned into two contrast. One contrast, larger in size, have primary FCC solid solution and other, smaller in size have eutectic phase composed of FCC solid solution and Laves phase.

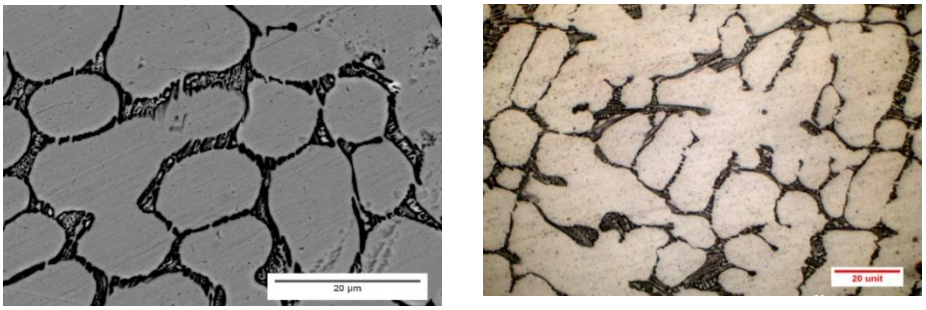

Figure 14**:** (a) SEM Image at 2000X and (b) Microscopic Image at 1600X at Zr = 2.5 at%

Zr=5.0%

When Zr=5 at% was added to the HEA then the given below SEM image is clearly revealing two contrast as similar to HEA with 2.5 at% of Zr but the contrast size of eutectic phase is found to be increased, and contrast size of FCC solid solution decreased. This is due to the increased concentration of Zr

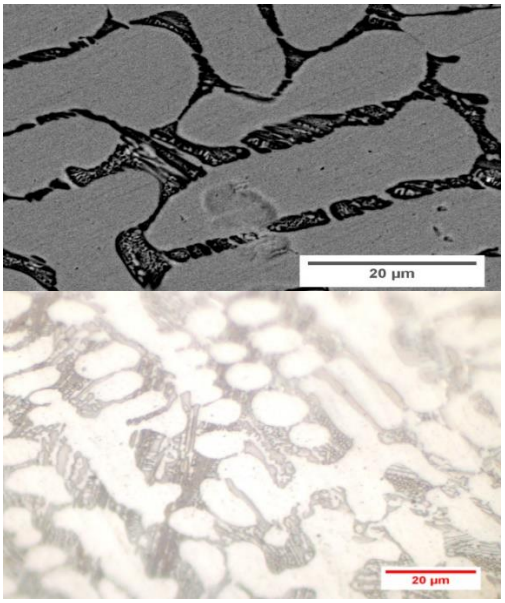

Figure 14**:** (a) SEM Image at 2000X and (b) Microscopic Image at 1600X at Zr = 5.0 at%

Zr=7.5%

Now 7.5 at% of Zr was added to the HEA and observed under SEM in a backscattered mode which has been shown in given below figure. The SEM image is clearly revealing that the microstructure is composed of three contrast- primary FCC solid solution, Eutectic dual phase mixture and Zr-rich solid solution, but the contrast size of primary phase is significantly reduced.

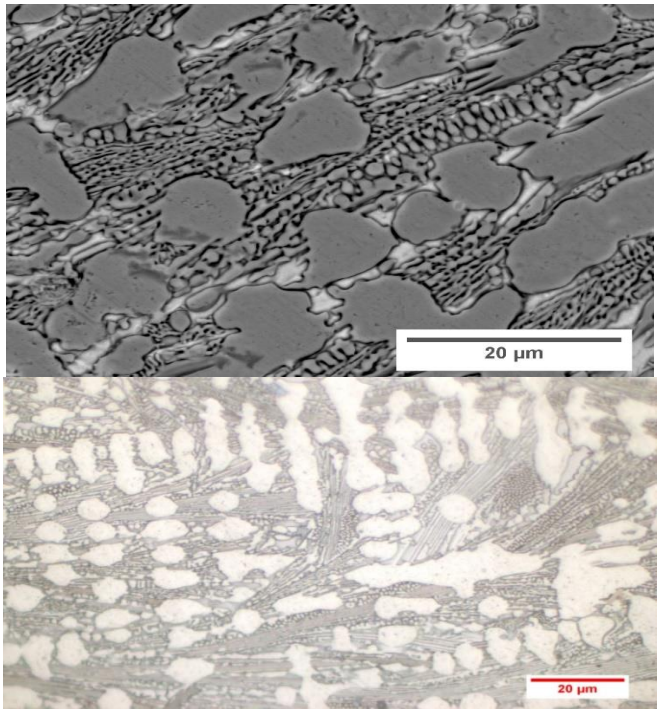

Figure 15**:** (a) SEM Image at 2000X and (b) Microscopic Image at 1600X at Zr = 7.5 at%

Zr=10%

Finally, when Zr=10 at% was added to the HEA, then the observed SEM image, as shown in the given below the figure, is turned into a complete eutectic phase mixture.

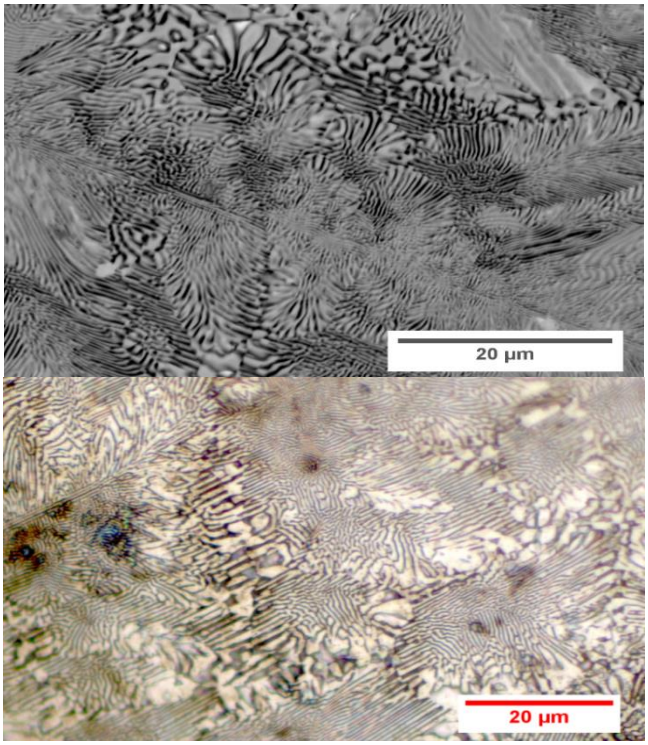

Figure 16 **:** (a) SEM Image at 2000X and (b)Microscopic Image at 1600X at Zr = 10 at%

X-Ray Diffraction

Diffraction patterns for every phase is as unique as our fingerprint. Phases with the same chemical composition can have drastically different diffraction patterns. The XRD patterns of the $(Fe_{25}Co_{25}Ni_{25}Cr_{20}V_5)_{100-x}Zr_x$ HEAs series are shown in the given below Fig 17, which have different zirconium (Zr) contents, that shows the different intense diffraction peaks to understand the structural Characterization.

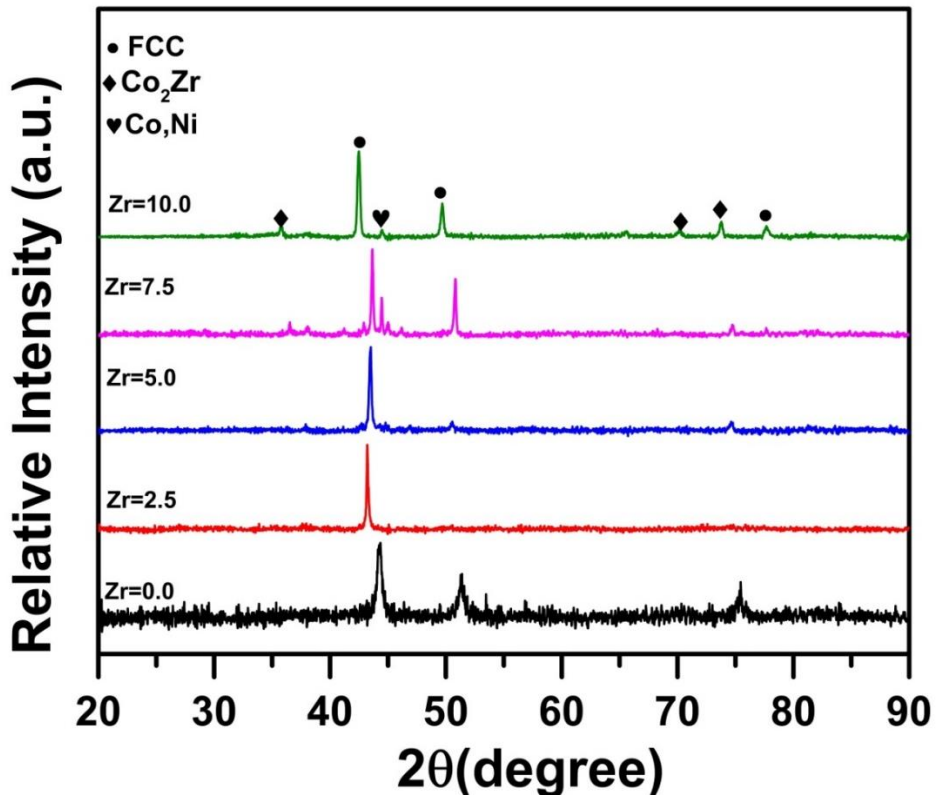

Figure 17: X-Ray Diffraction Patterns HEAs at Zr = 0, 2.5, 5.0, 7.5 and 10 at%

The results show that $(Fe_{25}Co_{25}Ni_{25}Cr_{20}V_5)_{100-X}Zr_X$ (x =0 at%) HEA possess a single FCC solid solution and on the addition of zirconium contents (x = 2.5, 5, 7.5 at. %), HEA starts forming a Laves phase (CoZr type) from liquid along with the FCC solid solution phase, as shown in the above Fig. Further, the XRD pattern gives another intermetallic phase (CoNi type) on the increasing zirconium (y = 10 at. %) contents, where (CoNi type) phase releases the lattice distortion energy when the zirconium (Zr) contents exceed the solution limit. The severe lattice distortion may reduce the intensity of diffraction peaks.

5.2 Corrosion Result

The potentiodynamic polarization curves of $(Fe_{25}Co_{25}Ni_{25}Cr_{20}V_5)_{100-x}Zr_x$ (x =0 at%) HEA in different solutions (water, seawater, 3M NaCl, 3M NaOH, and 3M HCl) and IS2062 in seawater are shown in Fig, and their electrochemical parameters corrosion current density (i_{corr}), corrosion potential (E_{corr}) and corrosion rate are listed in Table. The polarization curve of HEA and IS2062 are not overlapping each other; therefore, both are showing almost unlike corrosion-resistant behaviour. The potentiodynamic polarization curve for the HEA is showing lower corrosion current density (i_{corr}), higher corrosion potential (E_{corr}) as compared to IS2062 steel. Hence the HEA is having higher corrosion resistant than that of IS2062 steel which is also getting confirmed from Corrosion Rate (CR) values listed in the table.

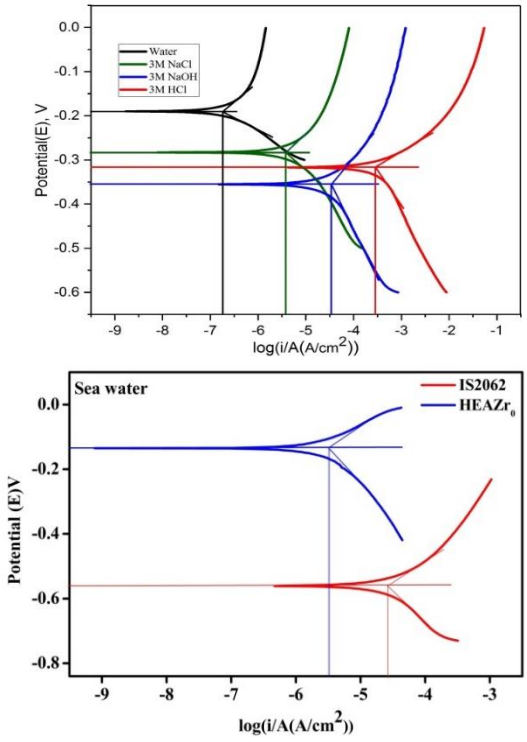

Figure 18**:** Potentiodynamic Polarization Curves for HEA at Zr = 0 at% Steel IS2062

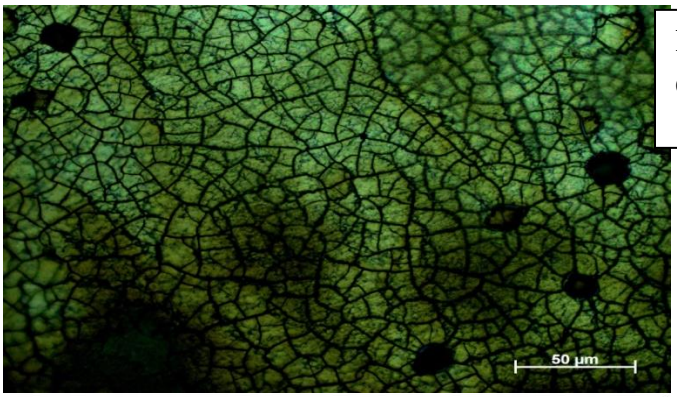

Figure 18a: Optical Image of $FeCoNiCrVZr_0$ HEA in 1M HCl

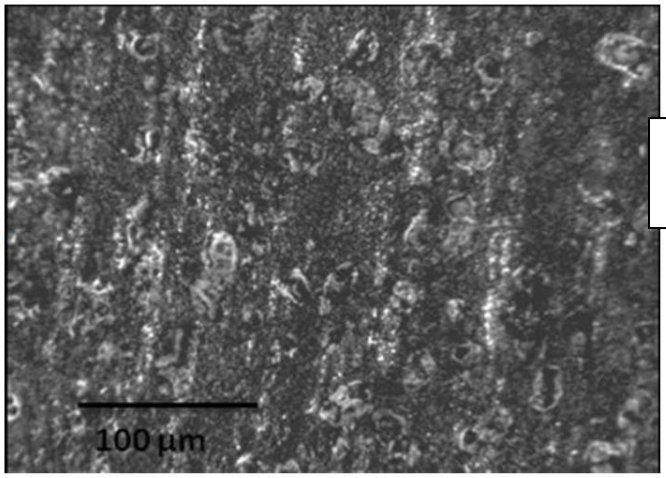

Figure 18b: Optical Image of Mild Steel in 1M HCl

From the potentiodynamic polarization curve and the table, it is confirmed that when the nature of solutions are changing the Corrosion current density (i_{corr}), Corrosion Potential (E_{corr}) and Corrosion Rate (therefore resistant to corrosion) are getting changed. It has been found that when the solution changes from tap water to 3M NaCl and then to 3M NaOH and finally to the 3M HCl, for the HEA (Zr=0), the Corrosion current density and corrosion potential (E_{corr}) are increasing. Therefore, the corrosion resistance is decreasing.

Table 4: Electrochemical Parameters

Solution	**E_{corr} (V)**	**I_{corr} (A/cm2)**	**CR (mmpy)**
H_2O (HEA)	0.27909	$1.778x10^{-7}$	0.004
Sea Water (IS2062)	0.56035	$2.674x10^{-5}$	0.621
Sea Water (HEA)	0.13813	$3.261x10^{-6}$	0.074
3M NaCl (HEA)	0.27963	$4.432x10^{-6}$	0.1012
3M NaOH (HEA)	0.35101	$3.373x10^{-5}$	0.7663
3M HCl (HEA)	0.30909	$2.096x10^{-4}$	4.7663

Chapter 6

6.1 Conclusion

Based upon results and discussion on the developed HEAs, the following conclusion can be drawn:

I. The high entropy alloys have been successfully prepared by solidification technique.

II. Effect of Zr on the morphology of the HEA is studied by using thermodynamic and Hume Rothery parameters.

III. Microstructural analysis of Zr containing alloys is done. The microstructure of the HEAs is changed from single-phase (FCC solid solution) at Zr=0 at% to primary FCC solid solution phase and eutectic which is composed of FCC solid solution phase and Laves phase (CoZr type) at (Zr=2.5 at%, 5.0 at%, and 7.5 at%) to complete eutectic phase mixture at Zr=10 at.%..

IV. The corrosion resistance of the HEA at Zr=0 at% is decreasing when electrolyte solution is changed from water to 3M NaCl to 3M NaOH and finally to the 3M HCl. The developed Fe-Co-Ni-Cr-V HEA shows excellent corrosion resistant as compared to the conventional IS2062 steel

6.2 Future work

For completion corrosion analysis of the HEAs, the corrosion experiments and microstructural study after the corrosion experiments of the compositions Zr= 5.0 at% and 10 at% can be done to make a directional decision.

To make a complete picture of strength properties and fracture mechanism, further study in this direction can be done.

The production costs of these HEAs can be estimated to have a good understanding over its economy.

The above study will make us know its competitiveness with other materials having good space in modern human society. It will enable us to estimate its market and industrial space in modern human society.

Therefore, it can help to realize the two-fold goals of attaining physical intellectual and spiritual stature by the individual, the very much objective of the material world and almost every constitution, especially the Indian Constitution.

References

[1]Arnvig, P.E., & Bisgard, A.D. (1996). Determining the potential independent critical pitting temperature (CPT) by a potentiostatic method using the Avesta Cell. United States: NACE International.

[2]ASTM G1-03(2017)e1 Standard Practice for Preparing, Cleaning, and Evaluating Corrosion Test Specimens, ASTM International, West Conshohocken, PA, 2017.

[3]ASTM G150-13 Standard Test Method for Electrochemical Critical Pitting Temperature Testing of Stainless Steels, ASTM International, West Conshohocken, PA, 2013.

[4]Carranza, R. M., & Alvarez, M. G. (1996). The effect of temperature on the passive film properties and pitting behaviour of a FeCrNi alloy

[5]Chen, Y., Duval, T., Hung, U., Yeh, J., & Shih, H. (2005). Microstructure and electrochemical properties of high entropy alloys—a comparison with type-304 stainless steel. Corrosion Science, 47(9), 2257-2279.

[6]Y.Y. Chen, T. Duval, U.D. Hung, J.W. Yeh, H.C. Shih, Microstructure and electrochemical properties of high entropy alloys—a comparison with type-304 stainless steel, Corrosion Science, 47 (2005) 2257-2279.

[7]Y.L. Chou, Y.C. Wang, J.W. Yeh, H.C. Shih, Pitting corrosion of the high-entropy alloy Co1.5CrFeNi1.5Ti0.5Mo0.1 in chloride-containing sulphate solutions, Corrosion Science, 52 (2010) 3481-3491.

[8]Y.L. Chou, J.W. Yeh, H.C. Shih, The effect of molybdenum on the corrosion behaviour of the high-entropy alloys Co1.5CrFeNi1.5Ti0.5Mox in aqueous environments, Corrosion Science, 52 (2010) 2571-2581.

[9]J.H. Cleland, What does the pitting resistance equivalent really tell us?, Engineering Failure Analysis, 3 (1996) 65-69.

[10]Cost of Corrosion Study, NACE, 2014.

[11]P. Crook and D. Klarstrom, Introduction to Alloys Resistant to Aqueous Corrosion, ASM International, Materials Park, OH (2005).

[12]Ernst, P., & Newman, R. C. (2007). Explanation of the effect of high chloride concentration on the critical pitting temperature of stainless steel

[13]Frankel, G. (1998). Pitting corrosion of metals a review of the critical factors. Journal of the Electrochemical Society, 145(6), 2186-2198. 81

[14]Frankel, G. S., Li, T., & Scully, J. R. (2017). Perspective—localized corrosion: Passive film breakdown vs pit growth stability. Journal of the Electrochemical Society, 164(4), C180-C181.

[15]Gao, M.C. Chapter 11: Design of high-entropy alloys. In High-Entropy Alloys: Fundamentals and Applications; Gao, M.C., Yeh, J.W., Liaw, P.K., Zhang, Y., Eds.; Springer: Cham, Switzerland, 2016.

[16]B. Gludovatz, A. Hohenwarter, D. Catoor, E.H. Chang, E.P. George, R.O. Ritchie, A fracture-resistant high-entropy alloy for cryogenic applications, Science, 345 (2014) 1153-1158.

[17]M.A. Hemphill, T. Yuan, G.Y. Wang, J.W. Yeh, C.W. Tsai, A. Chuang, P.K. Liaw, Fatigue behavior of Al0.5CoCrCuFeNi high entropy alloys, Acta Materialia, 60 (2012) 5723-5734.

[18]G. Herbsleb, Der Einfluß von Schwefeldioxid, Schwefelwasserstoff und Kohlenmonoxid auf die Lochkorrosion von austenitischen Chrom-Nickel-Stählen mit bis zu 4 Massen-Molybdän in 1 M Natriumchlorid-Lösung, Materials and Corrosion, 33 (1982) 334-340.

[19]Y.-J. Hsu, W.-C. Chiang, J.-K. Wu, Corrosion behavior of FeCoNiCrCux high-entropy alloys in 3.5% sodium chloride solution, Materials Chemistry and Physics, 92 (2005) 112-117.

[20]Hur, D. H., & Park, Y. (2006). Effect of temperature on the pitting behavior and passive film characteristics of alloy 600 in chloride solution. Corrosion, 62(9), 745-750

[21]R.F.A. Jargelius-Pettersson, Application of the Pitting Resistance Equivalent Concept to Some Highly Alloyed Austenitic Stainless Steels, CORROSION, 54 (1998) 162-168.

[22]Jones, D. A. (1996). Principles and prevention of corrosion prentice hall. Saddle River, NJ

Kao, Y., Lee, T., Chen, S., & Chang, Y. (2010). Electrochemical passive properties of AlxCoCrFeNi (x=0, 0.25, 0.50, 1.00) alloys in sulfuric acids

[23]Kehler, B., Ilevbare, G., & Scully, J. (2001). Crevice corrosion stabilization and repassivation behavior of alloy 625 and alloy 22. Corrosion, 57(12), 1042-1065.

[24]G. Koch, J. Varney, N. Thompson, O. Moghissi, M. Gould, J. Payer, International Measures of Prevention, Application, and Economics of Corrosion Technologies Study, NACE, (2016).

[25]C.J. Kuehmann, G.B. Olson, Computational materials design and engineering, Materials Science and Technology, 25 (2009) 472-478.

[26]Laycock, N. J., & Newman, R. C. (1997). Localized dissolution kinetics, salt films and pitting potentials

[27]C.P. Lee, Y.Y. Chen, C.Y. Hsu, J.W. Yeh, H.C. Shih, The Effect of Boron on the Corrosion Resistance of the High Entropy Alloys Al0.5CoCrCuFeNiB x, Journal of The Electrochemical Society, 154 (2007) C424-C430.

[28]Lee, C. P., Chang, C. C., Chen, Y. Y., Yeh, J. W., & Shih, H. C. (2008). Effect of the aluminium content of AlxCrFe1.5MnNi0.5 high-entropy alloys on the corrosion behaviour in aqueous environments 82

[29]Li, C., Li, J. C., Zhao, M., & Jiang, Q. (2009). Effect of alloying elements on microstructure and properties of multiprincipal elements high-entropy alloys

[30]Z. Li, K.G. Pradeep, Y. Deng, D. Raabe, C.C. Tasan, Metastable high-entropy dual-phase alloys overcome the strength–ductility trade-off, Nature, 534 (2016) 227.

[31]J. Li, X. Yang, R. Zhu, Y. Zhang, Corrosion and Serration Behaviors of TiZr0.5NbCr0.5VxMoy High Entropy Alloys in Aqueous Environments, Metals, 4 (2014) 597.

[32]Q.H. Li, T.M. Yue, Z.N. Guo, X. Lin, Microstructure and Corrosion Properties of AlCoCrFeNi High Entropy Alloy Coatings Deposited on AISI 1045 Steel by the Electrospark Process, Metallurgical and Materials Transactions A, 44 (2013) 1767-1778.

[33]Li, X., Zheng, Z., Dou, D., & Li, J. (2016). Microstructure and properties of coating of FeAlCuCrCoMn high entropy alloy deposited by direct current magnetron sputtering. Materials Research, (AHEAD), 0-0.

[34]K. Lorenz, G. Medawar, Über das Korrosionsverhalten austenitischer Chrom-Nickel-(Molybdän-) Stähle mit und ohne Stickstoffzusatz unter besonderer Berücksichtigung ihrer Beanspruchbarkeit in chloridhaltigen Lösungen, Thyssenforschung, 1 (1969) 97-108.

[35]Marcus, P. (1998). Surface science approach of corrosion phenomena. Electrochimica Acta, 43(1-2), 109-118.

[36]Newman, R. C., Foong Tuck Meng, , & Sieradzki, K. (1988). Validation of a percolation model for passivation of Fe-Cr alloys: I current efficiency in the incompletely passivated state

[37]H. Okamoto, The effect of tungsten and molybdenum on the performance of super duplex stainless steels, in: Proc. Conf. Application of Stainless Steels '92, 1992, pp. 360-369.

[38]Otto, F., Yang, Y., Bei, H., & George, E. P. (2013). Relative effects of enthalpy and entropy on the phase stability of equiatomic high-entropy alloys. Acta Materialia, 61(7), 2628-2638.

[39]Park, C., Rao, V. S., & Kwon, H. (2005). Effects of sigma phase on the initiation and propagation of pitting corrosion of duplex stainless steel. Corrosion, 61(1), 76-83.

[40]Qiu, X., & Liu, C. (2013). Microstructure and properties of Al2CrFeCoCuTiNix high-entropy alloys prepared by laser cladding

[41]V.M. Salinas-Bravo, R.C. Newman, Corrosion Science, 36 (1994) 67-77.

[42]L.J. Santodonato, Y. Zhang, M. Feygenson, C.M. Parish, M.C. Gao, R.J.K. Weber, J.C. Neuefeind, Z. Tang, P.K. Liaw, Deviation from high-entropy configurations in the atomic distributions of a multi-principal-element alloy, Nature Communications, 6 (2015) 5964.

[43]Schmuki, P. (2002). From bacon to barriers: A review on the passivity of metals and alloys. Journal of Solid State Electrochemistry, 6(3), 145-164.

[44]O.N. Senkov, S.V. Senkova, C. Woodward, Effect of aluminum on the microstructure and properties of two refractory high-entropy alloys, Acta Materialia, 68 (2014) 214-228. 83

[45]Y. Shi, B. Yang, X. Xie, J. Brechtl, K.A. Dahmen, P.K. Liaw, Corrosion of Al xCoCrFeNi high-entropy alloys: Al-content and potential scan-rate dependent pitting behavior, Corrosion Science, 119 (2017) 33-45.

[46]Shi, Y., Yang, B., & Liaw, P. K. (2017). Corrosion-resistant high-entropy alloys: A review. Metals, 7(2), 43.

Stellwag, B. (1997). Pitting resistance of alloy 800 as a function of temperature and prefilming in high-temperature water. Corrosion, 53(2), 120-128.

[47]Stepanov, N. D., Shaysultanov, D. G., Yurchenko, N. Y., Zherebtsov, S. V., Ladygin, A. N., Salishchev, G. A., & Tikhonovsky, M. A. (2015). High temperature deformation behavior and dynamic recrystallization in CoCrFeNiMn high entropy alloy

[48]Stockert, L., Hunkeler, F., & Bohni, H. (1985). A crevice-free measurement technique to determine reproducible pitting potentials. Corrosion, 41(11), 676-677.

[49]Z. Tang, T. Yuan, C.-W. Tsai, J.-W. Yeh, C.D. Lundin, P.K. Liaw, Fatigue behavior of a wrought Al0.5CoCrCuFeNi two-phase high-entropy alloy, Acta Materialia, 99 (2015) 247-258.